USGS
science for a changing world

Three-Dimensional Geologic Map of the Southern Carson Sink, Nevada, Including the Fallon FORGE Area

By Drew L. Siler, James E. Faulds, Jonathan M.G. Glen, Nicholas H. Hinz, Jeffrey B. Witter, Kelly Blake, John Queen, and Mark Fortuna

Pamphlet to accompany
Scientific Investigations Map 3437

2019

U.S. Department of the Interior
U.S. Geological Survey

U.S. Department of the Interior
DAVID BERNHARDT, Secretary

U.S. Geological Survey
James F. Reilly II, Director

U.S. Geological Survey, Reston, Virginia: 2019

Suggested citation:
Siler, D.L., Faulds, J.E., Glen, J.M.G., Hinz, N.H., Witter, J.B., Blake, Kelly, Queen, John, and Fortuna, Mark, 2019, Three-dimensional geologic map of the southern Carson Sink, Nevada, including the Fallon FORGE area: U.S. Geological Survey Scientific Investigations Map 3437, 22 p., 1 sheet, https://doi.org/10.3133/sim3437.

ISSN 2329–132X (online)

Contents

Figures

Tables

Map Sheet

Three-Dimensional Geologic Map of the Southern Carson Sink, Nevada, Including the Fallon FORGE area

By Drew L. Siler[1], James E. Faulds[2], Jonathan M.G. Glen[1], Nicholas H. Hinz[2], Jeffrey B. Witter[3], Kelly Blake[4], John Queen[5], and Mark Fortuna[6]

Abstract

The three-dimensional (3–D) geologic map characterizes the subsurface in the southern Carson Sink region. We created the 3–D map by integrating the results from seismic-reflection, potential-field-geophysical, and lithologic well-logging investigations completed in and around the Fallon FORGE site as part of the U.S. Department of Energy Frontier Observatory for Research in Geothermal Energy (FORGE) initiative from 2015–2018. The FORGE initiative was part of an effort to develop the technologies, techniques, and knowledge needed to make enhanced geothermal systems (EGS) a commercially viable electricity-generation option for the United States. Geologic units and structures mapped during the Fallon FORGE study, which particularly focused on the Mesozoic basement, were extrapolated to create the 3–D map of the southern Carson Sink area. The 3–D map area is 10 km wide along the east-west and north-south axes and extends 2.5 km below sea level, ~3.7 km below the land surface. Views of the map include horizontal and vertical sections and oblique perspective views from several angles. We describe the geologic units and structures and discuss the methods used to integrate the geologic and geophysical information in a 3–D geologic interpretation. We provide digital data for elements of the map, such as individual 3–D fault and stratigraphic surfaces and surface-fault traces. Input data are available from various data repositories through cited web links. A brief movie displaying the 3–D map is available at https://doi.org/10.3133/sim3437.

Purpose and Scope

From 2015 to 2018, the Fallon Frontier Observatory for Research in Geothermal Energy (FORGE) project was the focus of research associated with developing, testing, and improving enhanced geothermal systems (EGS) technologies and techniques. EGS relies on generation of permeability in hot but impermeable rock through a variety of subsurface engineering processes. The ultimate aim of EGS is to produce a fluid circulation system between a group of wells that can be used to generate electricity or to link newly generated permeability to an existing producing geothermal field (Tester and others, 2006). Estimates suggest that, if developed, renewable EGS resources could constitute a significant portion of future domestic energy needs in the United States (Tester and others, 2006; Blackwell and others, 2007; Williams and others, 2008). A detailed geologic understanding of the subsurface is critical to develop successful EGS. This 3–D geologic map (map sheet; also movie at https://doi.org/10.3133/sim3437) provides a subsurface characterization of the southern Carson Sink to inform the EGS research completed at the Fallon FORGE site.

The 3–D map area is in the southern Carson Sink, approximately 10 km south-southeast of the city of Fallon, Nevada (fig. 1), and includes the Fallon FORGE site, which is located predominantly on land owned by the Naval Air Station Fallon and on adjacent land owned and leased by Ormat Nevada, Inc. The Fallon FORGE site is a T-shaped area ~3.6 km (north-south) x 4.0 km (east-west) (fig. 2). Within this area, the Mesozoic basement section, in particular, was the primary subject of FORGE research (Blankenship and others, 2016; Ayling and others, 2018). Accordingly, the following geologic features were the focus of the geologic characterization: (1) the contact between the Mesozoic basement and the overlying Neogene strata, (2) the geometry and lithology of the different subunits within the Mesozoic basement, and (3) the geometries and relative ages of faults cutting the basement.

Introduction

The 3–D map and this report describe the subsurface geology and structure of a 10 km x 10 km area (100 km^2), encompassing the Fallon FORGE site, in the southern part of the Carson Sink (fig. 1). The geologic relations shown in the 3–D map are based on interpretations of geologic and geophysical

[1] U.S. Geological Survey
[2] Nevada Bureau of Mines and Geology
[3] Innovate Geothermal Ltd.
[4] Navy Geothermal Program Office
[5] Hi-Q Geophysical Inc.
[6] MAF Seismic LLC

data, as well as subsequent construction of geologic surfaces (for example, faults and geologic contacts) using 3–D interpolation algorithms.

The most detailed 3–D geologic characterization within the broader 100-km^2 area was constructed for the T-shaped Fallon FORGE site. This portion of the 3–D map, the Fallon FORGE area, is 3.6 km (north-south) by 4.0 km (east-west) and extends from the surface (~1,200-m elevation) to 2.5 km below sea level. The geologic features displayed in this area are supported by dense subsurface well data (fig. 2) that allow the top of the Mesozoic basement contact and the four lithologic units within the basement to be identified and mapped.

To constrain the geologic relations and fault structure within the broader context of the local basin architecture, subsurface data in the Fallon FORGE area were extrapolated to create the southern Carson Sink 3–D map (fig. 1). Because of the relative sparsity of deep well data outside of the Fallon FORGE area (fig. 2), the Mesozoic units are lumped into a single, undivided Mesozoic basement unit. All faults in the Fallon FORGE area seamlessly continue throughout the 3–D map.

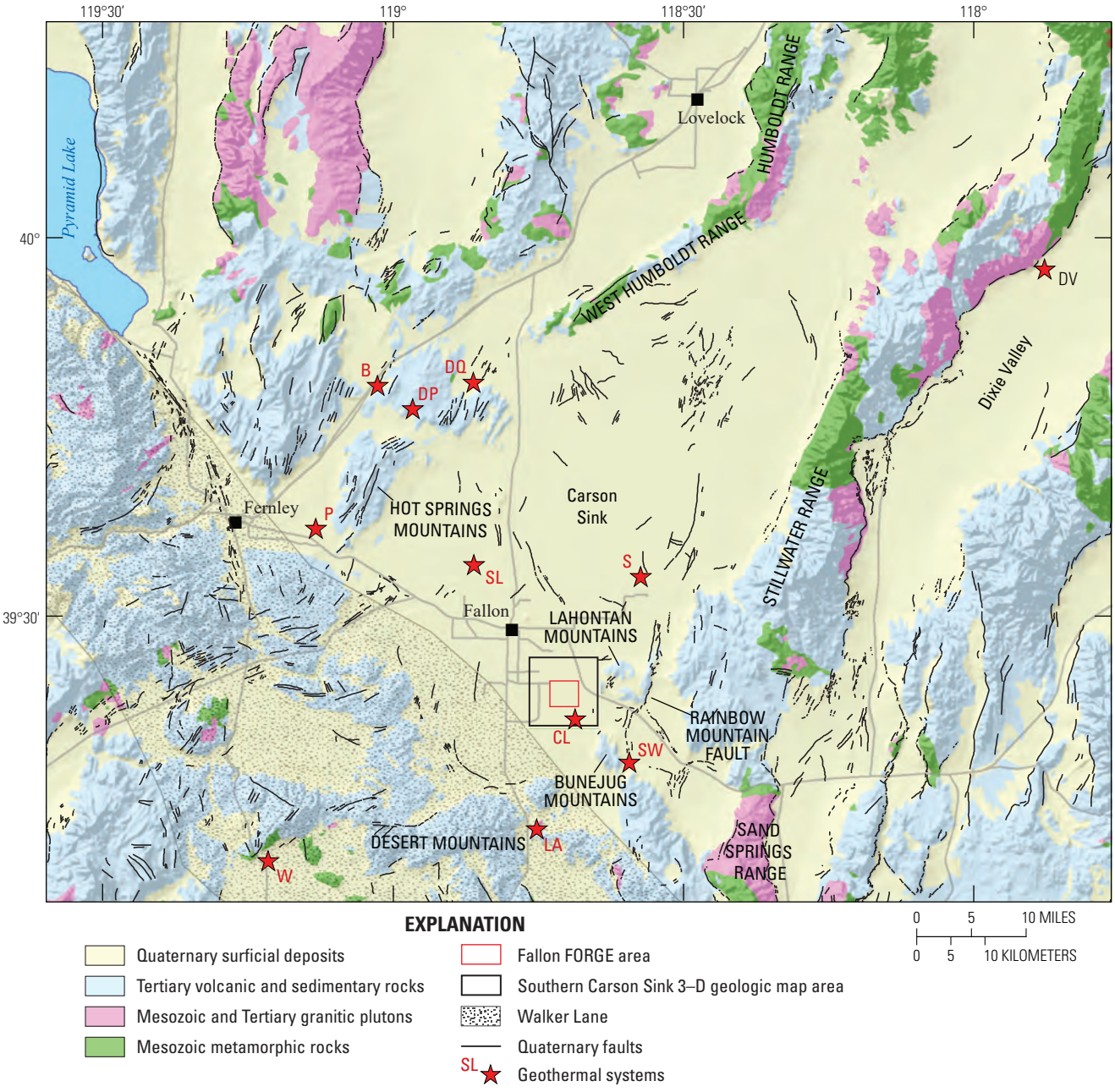

Figure 1. Regional map of Carson Sink area showing generalized bedrock geology (from Crafford, 2010) and location of southern Carson Sink 3–D map. Geothermal systems: B, Bradys; DP, Desert Peak; DQ, Desert Queen; DV, Dixie Valley; CL, Carson Lake; LA, Lee-Allen; P, Patua; S, Stillwater, SL, Soda Lake; SW, Salt Wells, W, Wabuska. Quaternary faults from U.S. Geological Survey Quaternary fault and fold database (U.S. Geological Survey, 2006). FORGE, Frontier Observatory for Research in Geothermal Energy.

The resulting 3–D geologic map displays subsurface fault surfaces, stratigraphic contacts, and rock volumes. The Fallon FORGE area retains the four subunits in the Mesozoic basement, but the Mesozoic basement is undivided outside of this area. The Neogene sedimentary and volcanic units overlying the Mesozoic basement are mapped consistently throughout the 3–D map.

Definition of the geologic and structural features of the 3–D map is supported by lithologic analyses of ~16,500 m of cores and cuttings from nine wells within the 3–D map area and twenty-four wells in the region surrounding the map (figs. 2, 3); geochemical analyses of Miocene volcanic units and Mesozoic metavolcanic units (fig. 4); seismic-reflection interpretation (figs 5, 6); interpretation of gravity anomalies and horizontal gravity gradients (figs. 5, 7); interpretation of magnetic anomalies and horizontal magnetic gradients (fig. 5, 8); two-dimensional (2–D) forward modeling of gravity and magnetic data (fig. 9); and structural analysis based on image logs from four wells within the map (figs. 2, 10). In addition to site characterization for EGS research, potential applications of this map include reservoir modeling, seismicity analysis, conventional geothermal exploration, education and scientific inquiry, and basin hydrogeology (see Potential Applications for 3–D Map section of this report).

Geologic Setting

Several major tectonic episodes affected the Carson Sink region and are relevant to the geologic structure and stratigraphy in the 3–D map area. The earliest tectonic event expressed in the southern Carson Sink is Mesozoic contraction with associated arc and back-arc volcanism and sedimentation. This contractional deformation includes low-grade metamorphism and folding and thrusting of the Mesozoic stratigraphy (for example, Page, 1965; Schweickert and Cowan, 1975; Stewart and Carlson, 1978; Satterfield, 2002; Hinz and others, 2008, 2010, 2014). Mesozoic tectonism and magmatism was followed by a period of uplift and erosion and later by eruption of regionally extensive rhyolitic ash-flow tuff sequences in the Oligocene (Henry, 2008; Henry and others, 2012). Regionally extensive, generally mafic volcanism associated with the ancestral Cascade Volcanic Arc followed in the Miocene (Wernicke and others, 1987; Cousens and others, 2008). Subsequent to the mafic volcanism, the Carson Sink underwent normal faulting associated with east-west to west-northwest Basin and Range extension from the early Miocene to the present (Colgan and others, 2006; Fosdick and Colgan, 2008). The southern and western parts of the Carson Sink experienced Walker Lane-type dextral shear deformation from late Miocene to present (Faulds and Henry, 2008).

Published geological, seismic reflection, and gravity interpretations delineate a series of half-graben and associated tilted fault blocks that define the structure of the Carson Sink basin and the surrounding mountain ranges (for example, Hastings, 1979; John, 1995; Faulds and others, 2010a, 2012, 2015, 2018; Hinz and others, 2011, 2014; Gray and others, 2013). The major normal faults controlling the half graben generally strike north-northeast and are associated with the Miocene to recent Basin and Range extension. Adjacent basins and tilted fault blocks include a series of extensional anticlines and synclines (Faulds and Varga, 1998).

A magnitude 6.9 dextral-normal earthquake in 1954 on the Rainbow Mountain Fault occurred ~10 km east of the 3–D map, illustrating that the Carson Sink region remains tectonically active to the present (Doser, 1986; Caskey and others, 2004). Accordingly, Quaternary faulting is common throughout the Carson Sink. However, detailed geologic mapping and analysis of lidar data within and adjacent to the map area suggest that no late Pleistocene to Holocene faults are found within the 3–D map area (fig. 1; Fallon area lidar data are available at https://gdr.openei.org/submissions/821, Sandia National Laboratories, 2017). The nearest Quaternary scarp lies ~1.5 km south of the southeast corner of the 3–D map and cuts late Pleistocene lacustrine sediments (Hinz and others, 2011). Though the U.S. Geological Survey Quaternary fault and fold database (U.S. Geological Survey, 2006) shows several Quaternary faults within and directly adjacent to the 3–D map (fig. 1), recent analysis suggests that these scarps are probably late Pleistocene shorelines rather than faults (J.W. Bell and N.H. Hinz, Nevada Bureau of Mines and Geology, unpublished data, 2011). The lack of late Pleistocene to Holocene faulting in the 3–D map area may indicate either a relatively tectonically quiescent period or may result from erosion or obscuring of fault scarps by processes associated with at least two lacustrine high-stands since ~13 Ma (Bell and others, 2009; Bell and House, 2010).

Data

Well Cuttings and Cores

Data from thirty-three wells within and adjacent to the southern Carson Sink 3–D map were used to construct the map (fig. 2). Approximately 16,500 m of cores, spot cores, cuttings, and thin sections of core and cuttings were analyzed. Cores were evaluated by hand lens, and cuttings were examined in detail under a high-power binocular microscope. Petrographic thin sections collected at ~30-m intervals are available for several wells. The thin sections were used in conjunction with the physical cores and cutting samples to confirm lithologic data. The contacts between lithologic units (fig. 3) are based on these data (Hinz and others, 2016).

Late Miocene to Quaternary basin-fill sediments (unit QTs) are 0 to 1,400 m thick and thicken to the west, away from the hinge zone of an extensional anticline (figs. 6, 9). No contact in the Neogene sedimentary section is evident in the down-hole lithologic analyses (fig. 3), so this section is shown as a single unit (QTs) on figure 3. A prominent reflector is evident in the seismic-reflection data and is inferred to be a late Pliocene surface (fig. 6). This, rather than the lithologic data, allows for division of the Neogene sedimentary section into Quaternary and Tertiary sediments (QTs) and Tertiary sediments (Ts) in the 3–D map. The Neogene sedimentary section overlies Miocene

volcanic and lesser interbedded sedimentary rocks. This Miocene volcanic section is 700 to 1,100 m thick and is dominated by Miocene basaltic andesite lavas (figs. 3, 4) but includes four other volcanic rock types distinguished in the cuttings and core: volcanic breccia, lithic tuff, rhyolite and dacite, and andesite. These units correlate with mapped units in the Bunejug and Lahontan Mountains (Bell and House, 2010; Bell and others, 2009; Hinz and others, 2011). In the 3–D map, these units are lumped into Miocene volcanic rocks, undivided (unit Tvs) for two reasons: (1) it is not possible to correlate the subunits between wells throughout either the Fallon FORGE area or the southern Carson Sink 3–D map and (2) the focus of the project at the Fallon FORGE site was geologic characterization of the Mesozoic basement section, so, whereas precise definition of

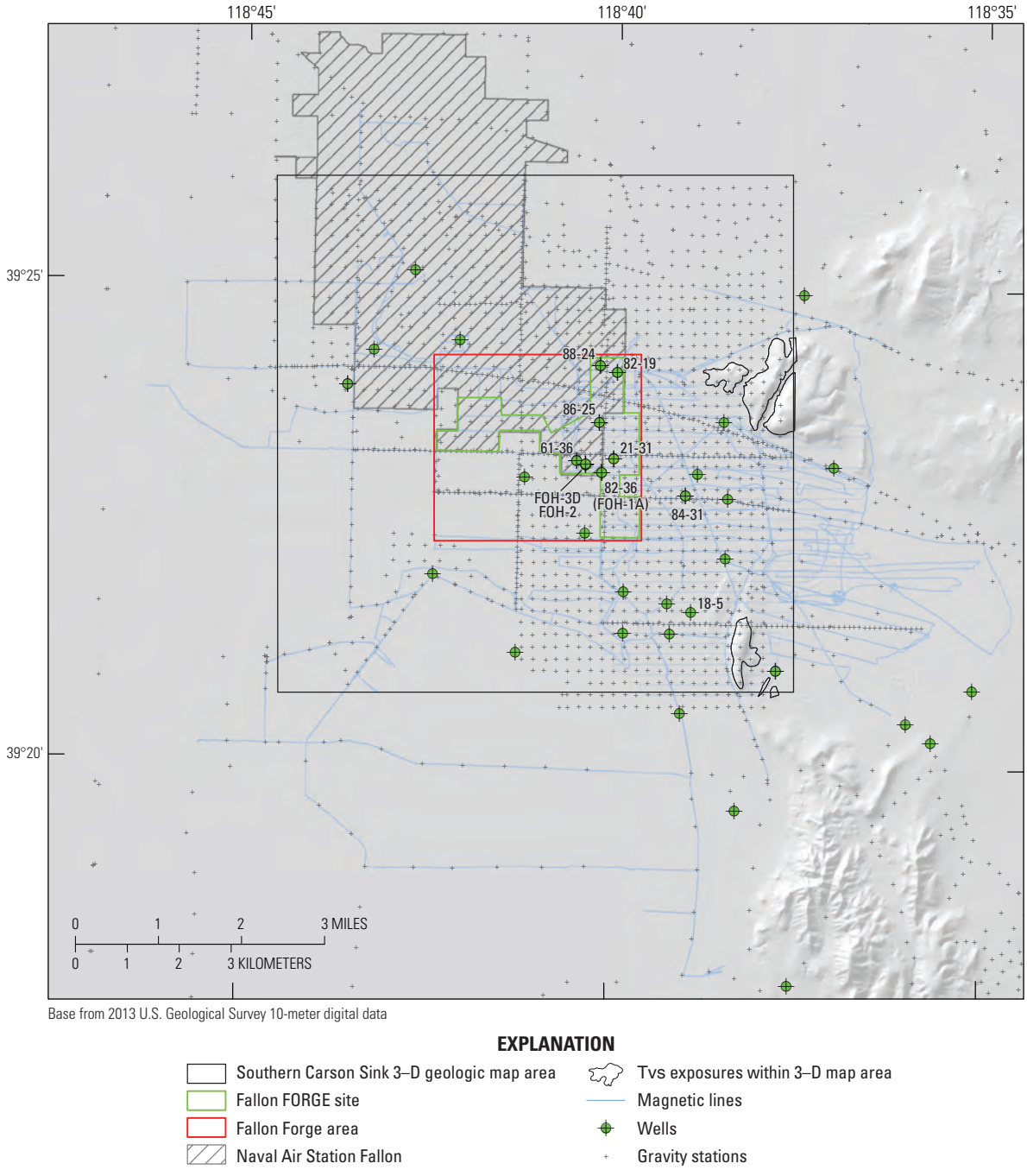

Figure 2. Southern Carson Sink area showing the locations of magnetic data and gravity stations used in construction of the 3–D map. The labeled wells contributed bedrock lithologic data (fig. 3) and (or) structural data (fig. 10). Other wells contributed temperature data or shallow geologic data (unconsolidated sediments). Lithologic information and faults mapped in unit Tvs exposures (Morrison, 1964; Bell and House, 2010; Hinz and others, 2011) are incorporated into the map. Hillshade from 10-m DEM, U.S. Geological Survey, 2013, USGS NED n40w119 1/3 arc-second. FORGE, Frontier Observatory for Research in Geothermal Energy.

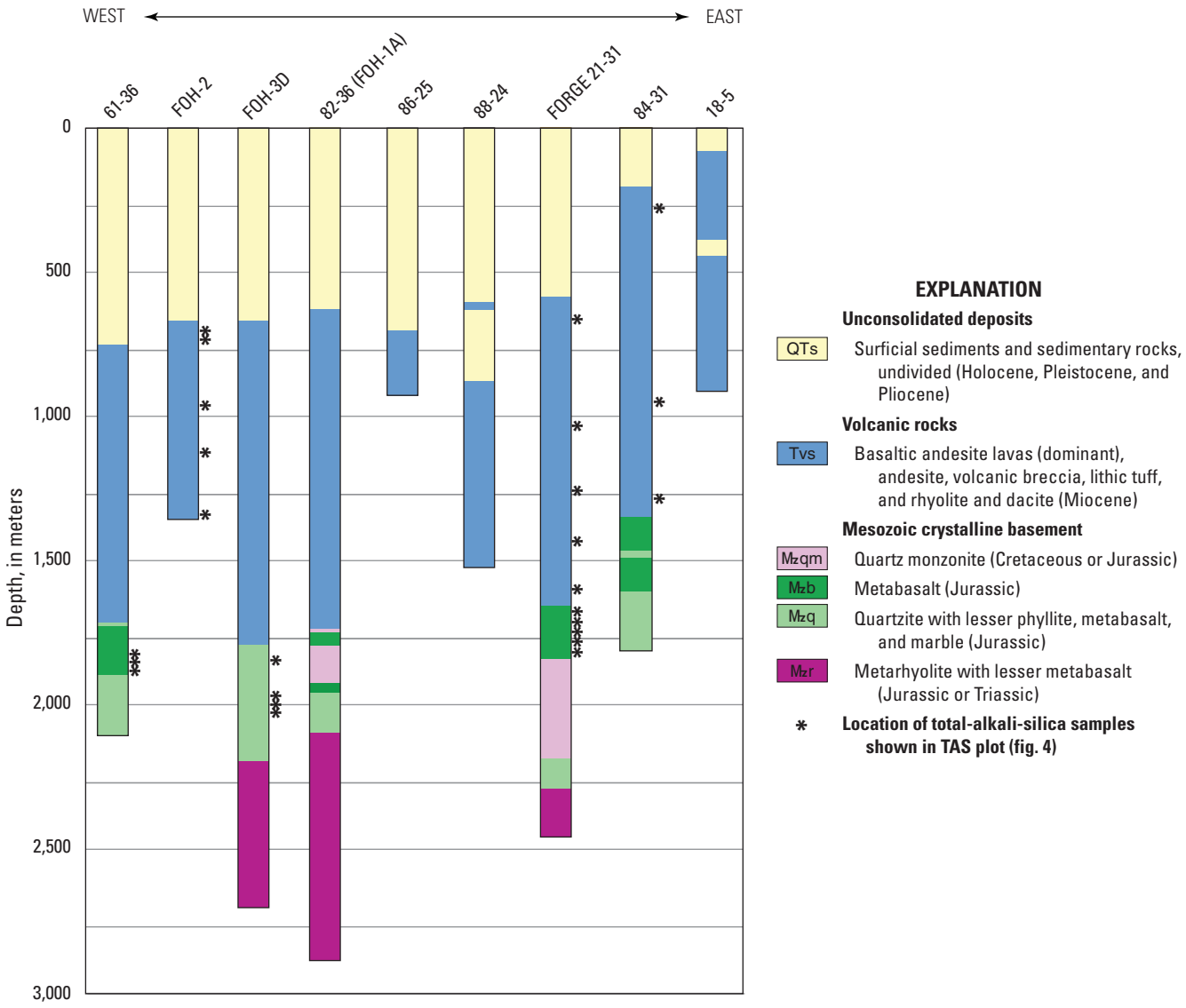

Figure 3. Graph showing lithologic logs from nine wells in the southern Carson Sink area (locations shown on fig. 2). In this figure, depth corresponds to well-path distance measured from the Kelly bushing—not true vertical depth. Wells are displayed right-to-left as they are located east-to-west on figure 2. The Mesozoic basement units are displayed divided in the Fallon FORGE area of the 3–D map and undivided as unit Mzu in the southern Carson Sink 3–D map. See detailed unit descriptions in the Description of Map Units. Asterisks along well path indicate locations of samples for total alkali silica (TAS) plot (fig.4). FORGE, Frontier Observatory for Research in Geothermal Energy.

the base of the Tertiary volcanic units was critical to project goals, the division of units within the overlying Neogene section was not. The westward-thickening Neogene sedimentary section suggests syntectonic deposition. The Miocene volcanic section (unit Tvs) remains close to 1 km thick throughout the 3–D map area (fig. 3), suggesting that the accumulation of these units preceded significant extension and basin subsidence.

The Miocene volcanic section rests nonconformably on heterogeneous Mesozoic basement. The Mesozoic basement, the focus of the geologic characterization at the Fallon FORGE site (Blankenship and others, 2016; Ayling and others, 2018), consists of low- to medium-grade Jurassic to Triassic metavolcanic and metasedimentary rocks that are locally intruded by as much as 130 m of quartz monzonite, which is likely Cretaceous or Jurassic (unit Mzqm, fig. 3). The upper part of the basement consists of predominantly metabasalt to metabasaltic andesite (unit Mzb), probably Jurassic, as much as 230 m thick. The underlying section consists of quartzite interlayered with lesser phyllite, metabasalt, and marble (unit Mzq) ranging from 100 to 380 m thick, which is also probably Jurassic. Metarhyolite ash-flow tuffs are locally interlayered with metabasalt (unit Mzr). Unit Mzr exceeds 790 m thick, is probably Jurassic or Triassic, and forms the deepest part of the basement that is penetrated by the existing wells.

Within the Fallon FORGE area, four wells (61-36, FOH-3–D, 82-36, and 21-31) penetrate the Mesozoic basement section (figs. 2, 3). The contacts between these units are traceable, so units Mzb, Mzq, Mzr, and Mzqm are mapped separately in this area. Only one additional well (84-31) reaches the Mesozoic basement in the southern Carson Sink 3–D map, so the

Mesozoic basement was left undivided (Mzu) outside of the Fallon FORGE area. See the Description of Map Units for detailed unit descriptions for all units on figure 3 and the 3–D map. Lithologic data are available at https://gdr.openei.org/submissions/1027 (Sandia National Laboratories, 2018a).

To more precisely define the contact between the Miocene mafic volcanic section (Tvs) and the underlying Mesozoic low- to medium-grade metamafic volcanic rocks (Mzb), whole-rock-geochemistry data were collected from (1) Miocene surface outcrop samples, (2) known Miocene lavas in core and spot core in several wells, and (3) mafic lavas and (or) metamafic lavas both above and below the location of the inferred Miocene-Mesozoic contact, as interpreted from the core and cuttings in well 21-31. Well 21-31 was drilled as part of the Fallon FORGE project in February 2018 (Ayling and others, 2018). The known Miocene, known Mesozoic, and suspected Miocene and Mesozoic data from well 21-31 largely overlap on the total alkali silica (TAS) plot (fig. 4), so ultimately the geochemistry data are not effective in defining the Miocene-Mesozoic contact. The original lithologic interpretation from the core, spot cores, and cuttings was, therefore, used to define the contact between the base of the Miocene volcanics and the top of Mesozoic basement (fig. 3).

Seismic Reflection

Two seismic reflection datasets, totaling approximately 270 km of profile length spanning the southern part of the Carson Sink, help to constrain the stratigraphic and structural framework of the southern Carson Sink 3–D map area. Approximately 83 km of reflection profiles span the 3–D map (figs. 2, 6). The two data sets are (1) a legacy data set consisting of depth-migrated data available only as digital image files (detailed in Blankenship and others, 2016) and (2) a digital dataset (originally interpreted in Gray and others, 2013, and reinterpreted in Blankenship and others, 2016). As part of this study, the digital dataset was reprocessed and remigrated utilizing modern methods with the purpose of (1) improving the signal strength and coherency of the Neogene basin-fill sediments, the underlying Miocene volcanics, and Mesozoic crystalline basement rocks and (2) collapsing fault diffractions to improve identification and definition of faults within the study area (methods detailed in Ayling and others, 2018; Hinz and others, 2017). These data constrain basin architecture, thickness of major stratigraphic units, and location and spacing of faults (fig. 6; Hinz and others, 2017; Faulds and others, 2018; Ayling and others, 2018; Siler and others, 2018a).

The seismic-reflection data demonstrate that the 3–D map area forms a gently west tilted half graben cut by widely spaced (0.5–2.0 km) east- and west-dipping normal faults. Interpretation of surface fault traces based on gravity and magnetic anomalies and local maximum horizontal gradients of the gravity and magnetic data (figs. 7, 8) helped to define the location and strike of faults and to connect faults between the reflection profiles. Lithologic data from wells were utilized to identify reflectors associated with the top of the Miocene volcanics. The 2–D modeling of high-resolution gravity data (~100-m station

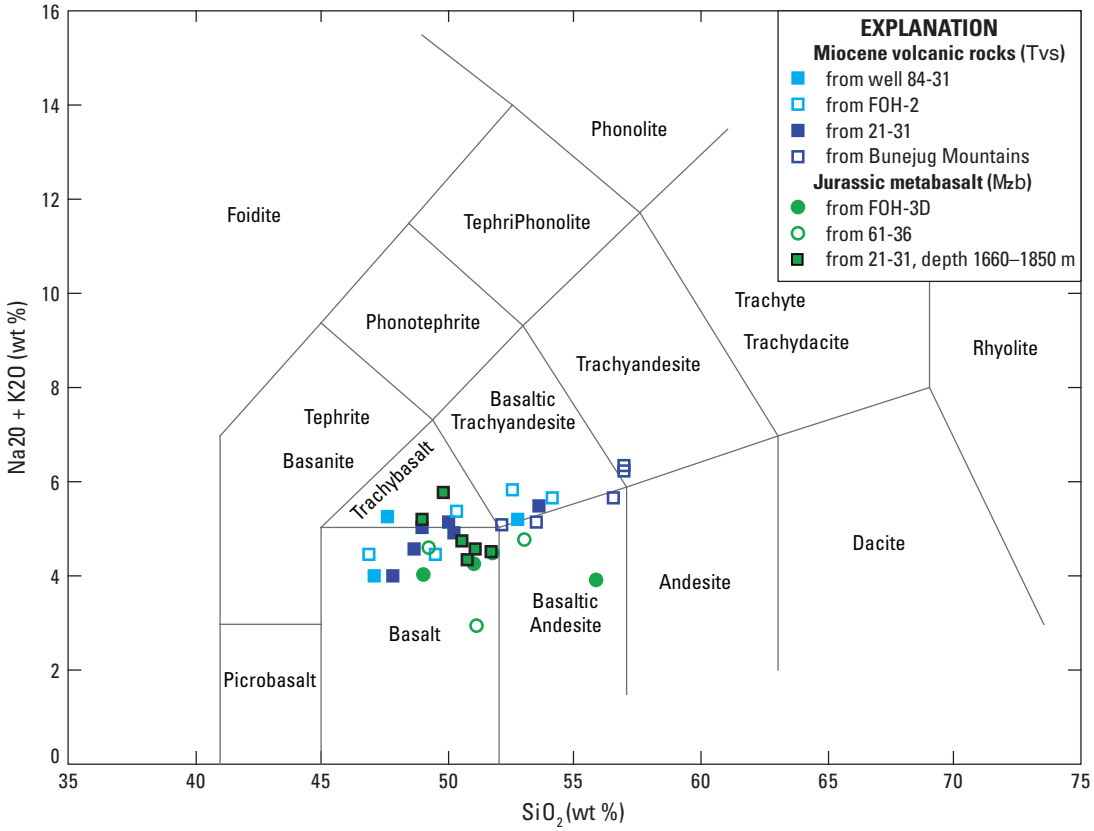

Figure 4. Total alkali silica (TAS) plot showing analyses of Miocene volcanic rocks (Tvs) and Jurassic metabasalt (Mzb) samples from wells in the Fallon FORGE area and the Bunejug Mountains. Sample locations along well paths are shown on figure 3.

spacing) combined with the seismic reflection was utilized to help constrain the depth to the base of the basin-fill sediments (for example, top of volcanic section). Due to relatively poor reflector coherence beneath the top of the Miocene volcanic section, the top of Mesozoic basement was largely interpreted from 2–D profile modeling of gravity data (figs. 6, 9). Three geologic contacts are apparent based on these analyses: the top of the Mesozoic basement, the top of the Miocene volcanic section, and a contact within the sedimentary section that we infer to be late Pliocene (fig. 6).

Faults, which are identified based on reflector truncation and integration of interpretations of the other datasets, dip moderately to steeply and accommodated relatively minor offset, typically ranging from approximately tens of meters to 200 m (fig. 6). Faults generally strike north to north-northeast, but several secondary fault populations (generally less than 100

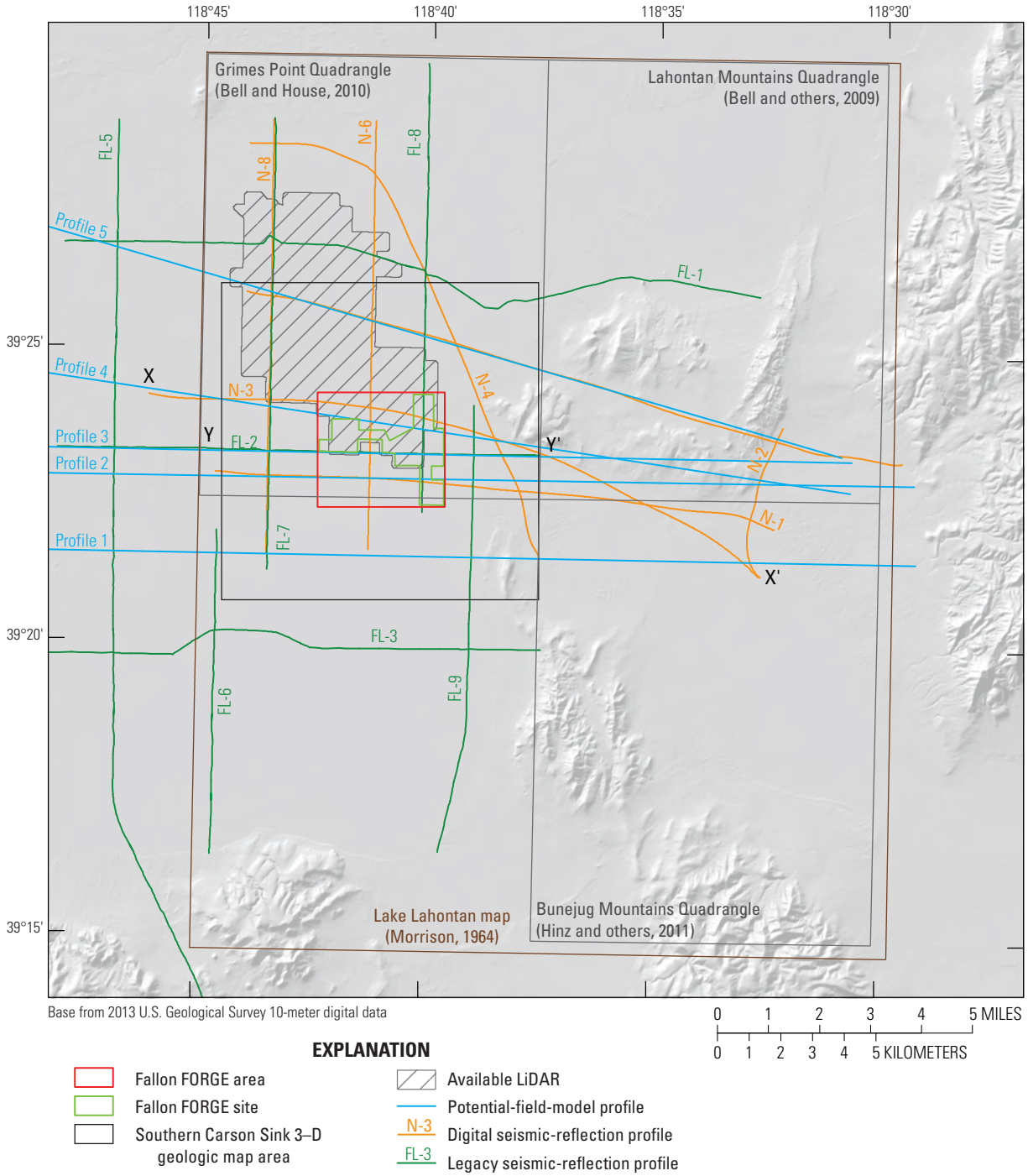

Figure 5. Map of southern Carson Sink area showing surface extents of southern Carson Sink 3–D map, Fallon FORGE area, and Fallon FORGE site, as well as locations of published geologic maps, available lidar, seismic-reflection data, and potential-fields-profile models used in construction of the 3–D map. Reflection profile N-3 (X–X') is shown on figure 6. Potential-field-modeling profile 3 (Y–Y') is shown on figure 8. Hillshade from 10-m DEM, U.S. Geological Survey, 2013, USGS NED n40w119 1/3 arc-second. FORGE, Frontier Observatory for Research in Geothermal Energy.

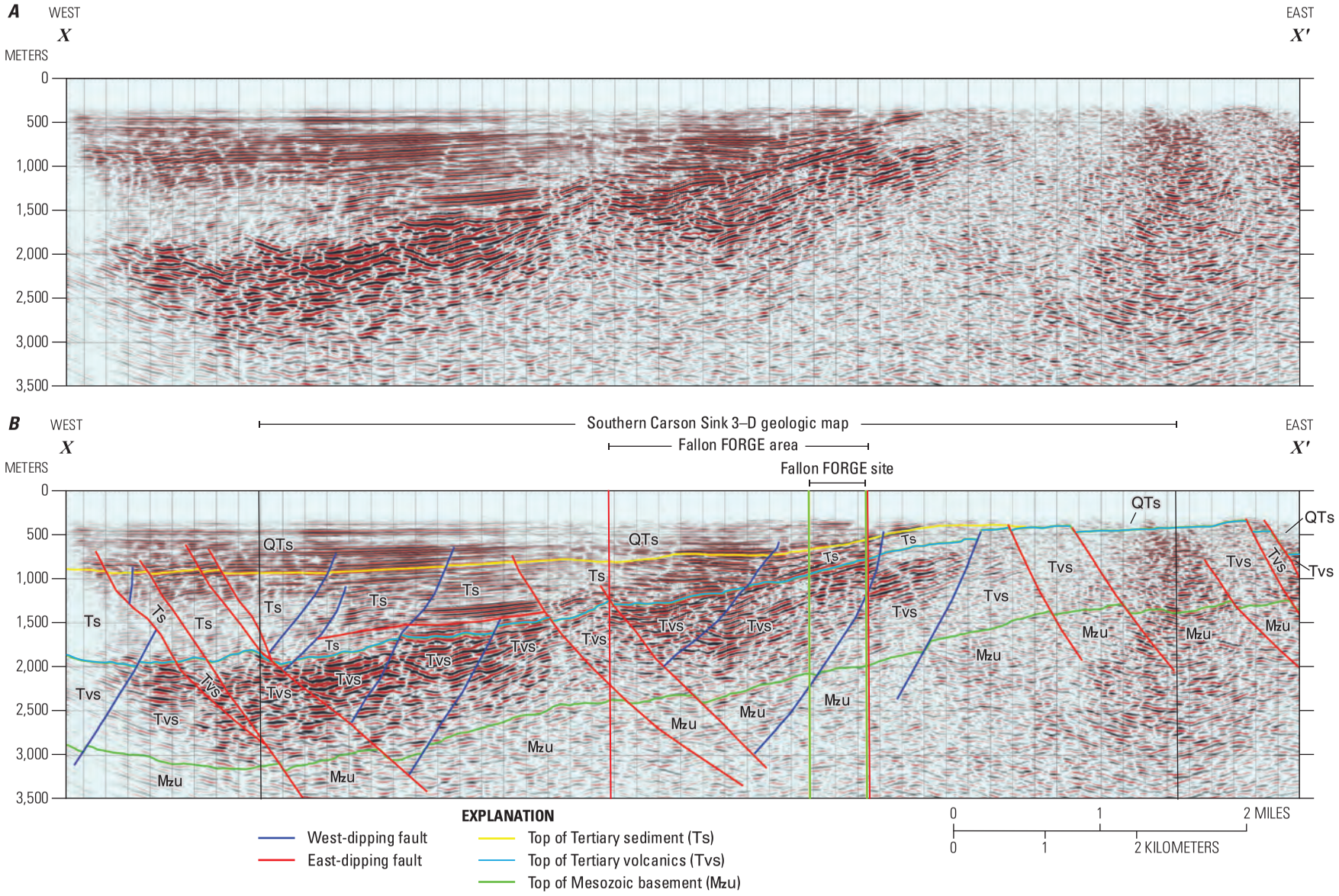

Figure 6. Seismic-reflection data (*A*) and interpretation (*B*) of Line N-3 (fig. 5, cross section X–X′). FORGE, Frontier Observatory for Research in Geothermal Energy.

meters offset) strike approximately east to east-northeast and north-northwest. Several faults were inititally interpreted based on large horizontal gradients in gravity and magnetics (figs. 7, 8, 9) and subsequently identified in the seismic reflection. The seismic-reflection data are available at https://gdr.openei.org/submissions/1011 (Sandia National Laboratories, 2018b).

Potential-Field Data

A database of more than 8,000 gravity stations that span the Carson Sink was analyzed to help constrain the 3–D geometries of geologic contacts and faults in the 3–D map. The 10-km x 10-km area of the 3–D map contains ~1,750 gravity stations, with a typical spacing of 250–300 m, though more densely spaced stations (100 m) occur along the seismic reflection profiles, providing higher resolution data along the 2–D potential-field-profile models (figs. 5, 9). The remaining 6,250+ stations are spaced at 400- to 1,600-m intervals spanning an approximately 130-km x 130-km region surrounding the 3–D map area and provide regional control. All gravity data were reduced to isostatic residual gravity anomalies using standard gravity methods (Blakely, 1995) that correct for multiple parameters, including Earth tides, instrument drift, latitude, elevation, Earth curvature, terrain, and crustal root.

Approximately 600 km of ground magnetic data with approximately 250-m line spacing (fig. 2) help characterize the 3–D geologic structures in the 3–D map. Standard processing of these data was applied to correct for diurnal variations of the field (Telford and others, 1990), and the data were filtered to remove anomalies associated with cultural noise, such as cars, culverts, fences, and power lines.

Isostatic gravity anomalies (fig. 7), reduced-to-pole magnetic anomalies (fig. 8), and the locations of local maxima in the horizontal gradients of gravity (fig. 7) and reduced-to-pole magnetic anomalies (fig. 8) were calculated (for example, Blakely, 1995). These maximum horizontal gradients help to define surface-fault traces and help to connect fault profiles interpreted from the seismic-reflection data (fig. 6) and 2–D potential-field-profile models (fig. 9).

The gravity signature within the 3–D map area is dominated by a gravity high to the east and a gravity low to the west that are associated with the hinge zone of an extensional anticline in the near surface to the east of the 3–D model and a deepening west-tilted half graben along the west limb of the anticline, respectively (fig. 7). Within these broad anomalies, many local maximum horizontal gravity gradients are evident. Steep gradients in the gravity signal are associated with relatively large lateral density contrasts in the subsurface. Many of these maximum horizontal gradients correlate with faults interpreted from the seismic-reflection data and (or) mapped in the adjacent ranges.

Similar to the gravity data, the reduced-to-pole magnetic anomaly data also demonstrate a relatively strong magnetic field in the east and a relatively weak magnetic field in the west. Also similar to the gravity data, this signal is associated with the shallow hinge of the extensional anticline to the east and the deepening basin to the west. Several of the maximum horizontal magnetic gradients correlate with faults interpreted from the seismic-reflection data, maximum horizontal gravity gradients, and mapped faults in the adjacent ranges (fig. 8).

Two-dimensional (2–D) potential-field models were developed along five profiles across the 3–D map area (figs. 5, 9). The purpose of the 2–D potential-field-profile modeling is to (1) provide constraints on the locations of the major geologic contacts to integrate with the seismic-reflection interpretation, (2) add additional profile constraints on the locations of geologic contacts where seismic-reflection data are unavailable, and (3) constrain the locations of major faults. Commercially available software (GM-SYS®) was used to model the five profiles. The software employs standard forward-modeling methods (Talwani and others, 1959; Blakely and Connard, 1989) that approximate subsurface geology with horizontal tabular prisms characterized in the 2–D cross section as model blocks. The geometries of the model blocks are determined through a series of forward and inverse calculations (whereby density and magnetic properties of 2–D bodies are adjusted iteratively) to match model anomalies with observed anomalies within limits imposed by surface geology, rock property data, and maximum horizontal gradients. Rock density (325 samples), magnetic susceptibility (357 samples), and magnetic remanence (93 samples) data from core samples, paleomagnetic cores, and representative hand samples collected form the Bunejug and Lahontan Mountains (data available at https://gdr.openei.org/submissions/990, Sandia National Laboratories, 2017) are used in conjunction with data derived from a national database (D. Ponce, USGS, written commun., 2016) consisting of over 19,000 measurements made on lithologies similar to those in the 3–D map area. These data constrain the density and magnetic susceptibility of rock units in the 2–D potential-field models (fig. 5, Profiles 1–5; fig. 9) (Ayling and others, 2018).

The Quaternary and Neogene sedimentary section (QTs and Ts) is separated into four regionally extensive horizontal internal units (fig. 9; table 1). The density of each subunit increases with depth to reflect typical density-depth relations found in basins throughout Nevada (Jachens and Moring, 1990). A similar approach was used for the underlying volcanic section (Tvs). The four horizontal density sub-units in the volcanic section increase in density with depth, though they remain within the range of densities measured on the core and outcrop samples. Both normal and reversed magnetic-polarity Tvs units in the shallow subsurface are needed to fit the high-amplitude magnetic signal (fig. 9). Similarly, reverse- and normal-polarity Miocene mafic lava sections are exposed to the east of the 3–D map (Hinz and others, 2011, and unpublished data). The horizontal density layers in the Quaternary and Neogene sediments (QTs and Ts) and Miocene volcanic rocks (Tvs) represent realistic density-depth variation in the Earth's crust and provide a good fit between the profile model, the density measurements, and gravity measurements. These horizontal density layers are not correlated with any identified lithologic variation, and they are not incorporated in the 3–D geologic map. The location of the contact at the top of the Miocene volcanics (Tvs) throughout the 3–D map is defined by iterative comparison and adjustment of the contact interpreted from seismic-reflection data and the potential-field-profile models. Because the resolution of the seismic-reflection data below the upper contact of the Miocene

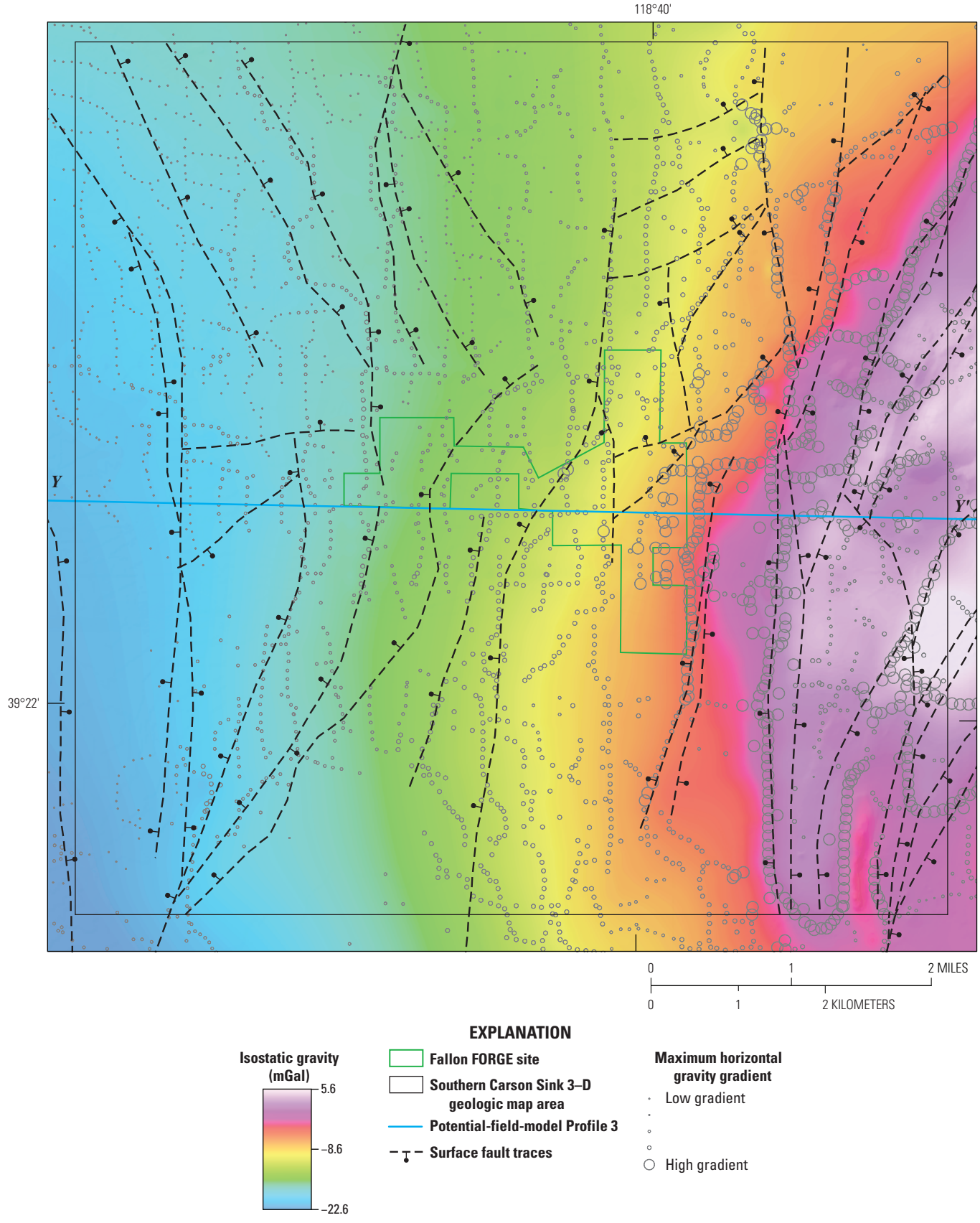

Figure 7. Map showing isostatic gravity in the area of the southern Carson Sink 3–D map. Warm colors indicate high gravity, cool colors low gravity. Surface traces of the fault planes in the 3–D map are shown. FORGE, Frontier Observatory for Research in Geothermal Energy.

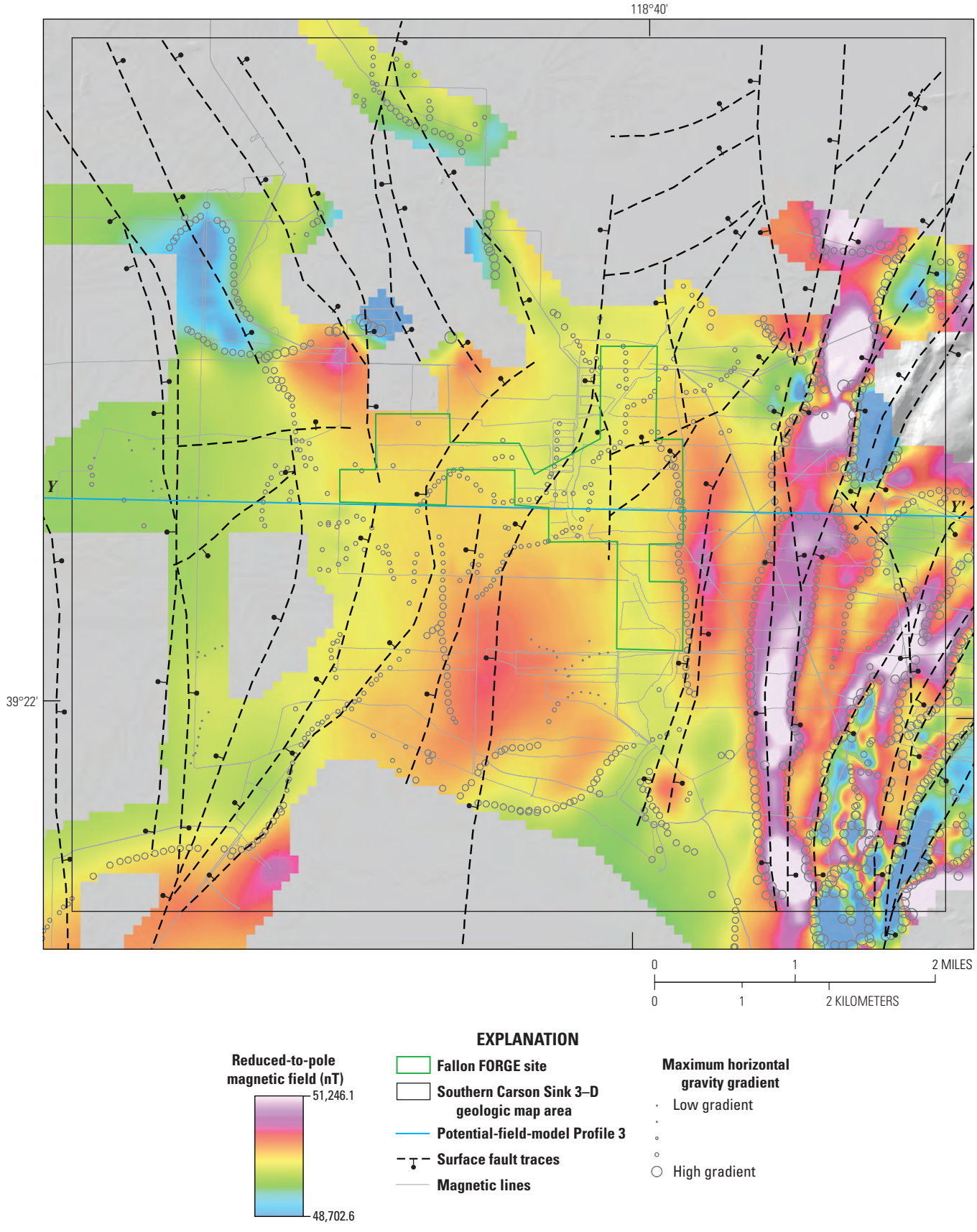

Figure 8. Map showing reduced-to-pole magnetic anomaly in southern Carson Sink 3–D map area. Warm colors indicate strong magnetic field; cool colors reflect a weak magnetic field. Surface traces of the fault planes in the 3–D map are shown. FORGE, Frontier Observatory for Research in Geothermal Energy.

Table 1. Magnetic and density properties used in potential-field modeling (fig. 9).

[Hyphen, no values were used in the model. Colors correspond to density subunits in potential-filed-profile model (fig. 9)]

Geologic map unit	Potential-field-model-unit	Density (kg/m³)	Magnetic susceptibility (SI)	Magnetic remanence (A/m)	Declination (deg)	Inclination (deg)
QTs and Ts	Sed1	1,900	0.002	0.0	-	-
	Sed2	2,000	0.007	0.0	-	-
	Sed3	2,200	0.005	0.0	-	-
	Sed4	2,300	0.0	0.0	-	-
(reversed polarity)	Volc1r	2,300	0.02	2.0	153	−30
Tvs	Volc1n	2,300	0.02	2.0	0.0	60
	Volc2	2,350	0.02	2.0	0.0	60
	Volc3	2,400	0.02	2.0	0.0	60
	Volc4	2,420	0.02	2.0	0.0	60
Mzu	Mzu	2,670	0.01	2.0	-	-

volcanic rocks (Tvs) is poor (fig. 6), the top of the Mesozoic basement is largely based on the potential-field modeling rather than the seismic-reflection profiles.

Distinct faults are not shown in the potential-field-profile models, but the likely locations of faults are indicated by adjacent lithologies of different density and (or) magnetic properties compared to the locations of faults interpreted from the other data sets and adjusted as necessary to iteratively develop an internally consistent structural interpretation. Potential-field data are available at https://doi.org/10.5066/F7J38RVZ (Phelps and Glen, 2018).

Methods

The southern Carson Sink 3–D map was constructed using the methods summarized below, which are similar to other recent contributions (Moeck and others, 2009, 2010; Faulds and others, 2010b; Jolie and others, 2012; 2015; Hinz and others, 2013a; Siler and Faulds, 2013; Siler and others, 2016a,b,c; Siler and others, 2018a). Commercially available software (EarthVision) was used for all 3–D work.

The 3–D fault interpretation is based on seismic-reflection interpretation, faults inferred from the 2–D potential-field-profile models, faults mapped adjacent to the 3–D map area, and fault traces interpreted from gravity and magnetic anomalies and gravity and magnetic horizontal gradients. Faults interpreted from the seismic-reflection profiles were compared to the mapped surface-fault traces adjacent to the 3–D model area, surface fault traces interpreted from the maximum horizontal gradients of gravity and magnetics, and faults indicated on 2–D potential-field-profile models, and their locations were adjusted as necessary. Faults evident from large gradients in the potential-field data, but not originally interpreted on the seismic reflection, are added to the seismic-reflection interpretation. A surface-fault-trace map was built by connecting 2–D fault profiles on the seismic-reflection profiles and 2–D potential-field profiles to those on neighboring profiles using the potential-field-anomaly maps and faults interpreted from gravity and magnetic maximum horizontal gradients. In this way, the 3–D fault interpretation was iteratively built to be consistent with all available data. The final fault profiles and surface traces were digitized or digitally added to the 3–D software environment, and 3–D fault surfaces were calculated based on these data.

Three-dimensional stratigraphic contacts were defined based on the bedrock exposures of Miocene volcanic rocks in the Lahontan and Bunejug mountains (figs. 1, 2; for example, Bell and House, 2010; Bell and others, 2009; Hinz and others, 2011; Morrison, 1964), downhole lithologic data interpreted from well cuttings and core (figs. 3, 4), interpretation of seismic-reflection profiles (fig. 6), and 2–D forward modeling of potential-field data (fig. 9). Similar to the faults, the 2–D profiles of the geologic contacts were iteratively refined between the seismic reflection, the down-hole lithologic data, the 2–D potential-field-profile models, and the 3–D fault surfaces to construct 3–D stratigraphic contacts consistent with all available data. The final stratigraphic contacts along the profiles were digitized or digitally added to the 3–D software environment.

Three-dimensional fault and stratigraphic surfaces were built from the input data using a minimum tension gridding algorithm provided within EarthVision software, which serves to generate relatively smooth surfaces while conforming to the input data. In areas of relatively sparse data, 3–D fault and stratigraphic surfaces were manually adjusted to retain strike and dip of both faults and contacts as constrained by the input data, as well as unit thickness and trends in thickness change as constrained by input data (for example, Siler and Faulds, 2013; Siler and others, 2016a,b,c; Siler and others, 2018a). Faults interpreted to not cut shallow stratigraphy are projected up-dip to the surface and displayed as dashed surface traces.

Following completion of the 3–D geologic map, 3–D geophysical inversion modelling of gravity data was completed (Witter and others, 2018). The purpose of this exercise was to test if the 3–D lithologic framework, assigned with representative values for rock density, is consistent with the observed

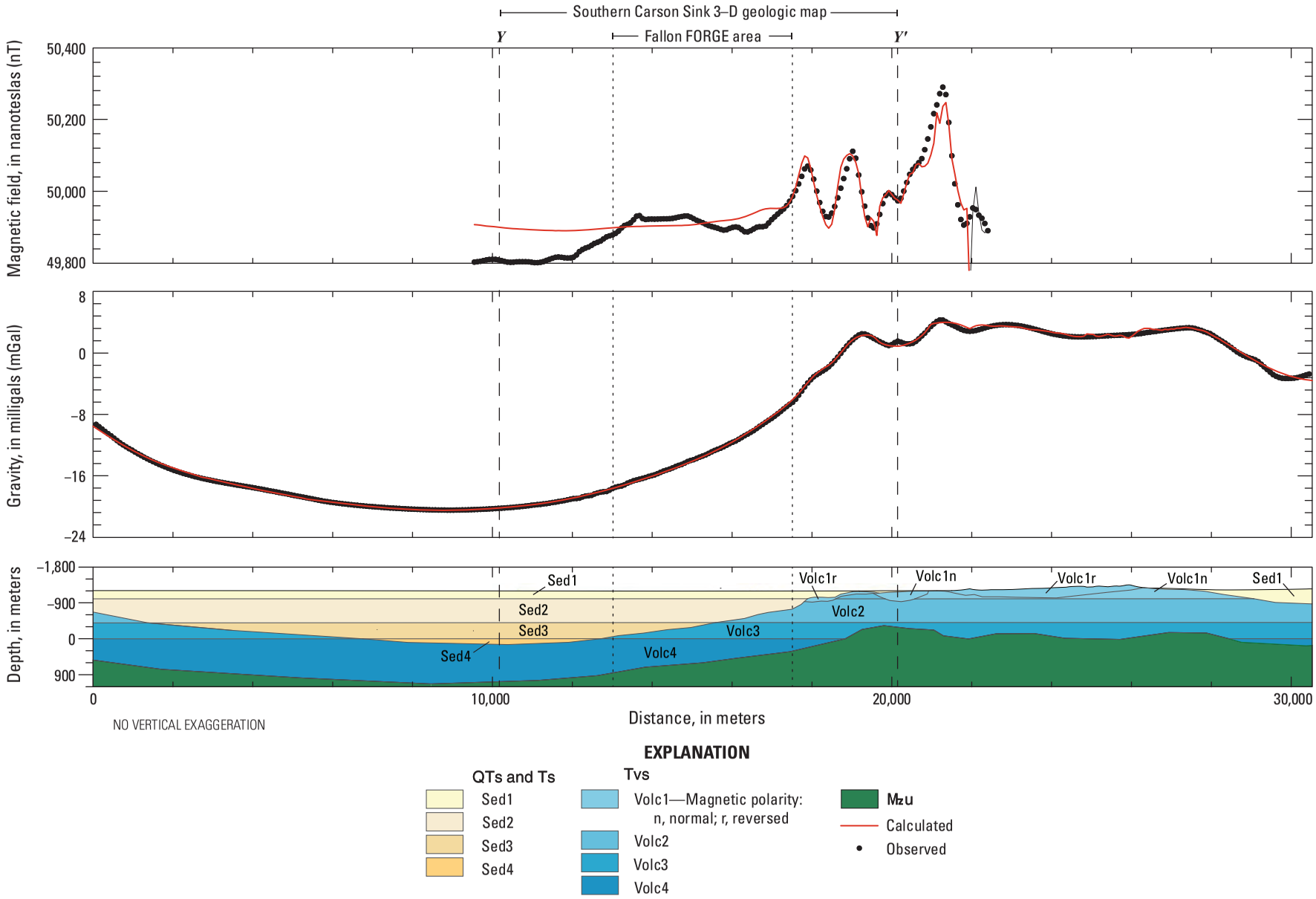

Figure 9. Potential-field-profile model for Profile 3 (see fig. 5 for location of Profile 3 and Y–Y′). Table 1 shows density and magnetic properties used in the model. Dashed lines indicate the boundaries of the southern Carson Sink 3–D geologic map; dotted lines the boundaries of the Fallon FORGE area. FORGE, Frontier Observatory for Research in Geothermal Energy.

gravity response across the entire 3–D map area; the 3–D map is shown to be largely consistent with the observed gravity. Relatively small degrees of misfit occur in the eastern portion of the 3–D map area, where more complex geology is present.

Mapping

The geologic units defined in the southern Carson Sink 3–D map area are units that may be reasonably mapped in three dimensions as constrained by the available data. In the structurally complex Carson Sink area, many individual geologic units shown in 1:24,000-scale maps (for example, Bell and others, 2009; Bell and House, 2010; Hinz and others, 2011) and 1:31,680-scale maps (Morrison, 1964) are lumped, rather than displayed individually, because insufficient data are available to map these individual units in three dimensions. In the 3–D map, the basin-fill sedimentary rocks are lumped into Quaternary–Tertiary sediments (QTs) and Tertiary sediments (Ts) that are distinguished by a prominent reflector in the seismic-reflection data (fig. 6) that we interpret to be late Pliocene. The Miocene volcanic rocks are lumped into one unit (Tvs), and the Mesozoic basement is lumped into one unit (Mzu). In the Fallon Forge area of the 3–D map, units QTs, Ts, and Tvs are consistent with the surrounding map area, whereas unit Mzu is divided into the four lithologic units defined from well cuttings and core analyses: (1) Cretaceous or Jurassic quartz monzonite (Mzqm), (2) Jurassic metabasalt (Mzb), (3) Jurassic quartzite (Mzq), and (4) Jurassic or Triassic rhyolite tuffs (Mzr).

Faults are mapped as individual normal fault surfaces of infinitesimal thickness. In reality, faults likely occur as zones of fracturing, brecciation, and fault gouge of varying thickness (Cowie and Scholz, 1992; Scholz and others, 1993; Anders and Wiltschko, 1994). For example, during drilling of well 21-31 in February 2018, minor lost circulation >20 barrels/hour occurred within ~200 m laterally of the westernmost (~100 m offset) west-dipping fault (map sheet, cross section C–C'), followed by larger lost circulation >113 barrels/hour at the bottom of the well, at the intersection of the well with the fault. The lost circulation at the bottom of the well is interpreted as local fracture permeability associated with the fault, whereas the minor lost circulation above may be related to a zone of fractured bedrock in the damage zone around the fault. Well 21-31 data are available at https://gdr.openei.org/submissions/1027 (Sandia National Laboratories, 2018a).

Alternatively, several of the 3–D mapped faults were penetrated by previous drilling and yielded no geologic evidence of faults in cuttings or core, as well as no lost circulation during drilling. Seismic-reflection data, potental-field modeling, and correlation of contacts in adjacent wells suggest relatively minor displacement (~200 m maximum) across the largest faults, including the fault intersected in 21-31, and significantly smaller offset (a few tens of meters) across the majority of faults. This information suggests that, although significant widths of fracturing may have developed around certain fault zones in the 3–D map area, the infinitesimal thickness is probably an appropriate approximation for most faults.

The relative proximity of the 3–D map area to documented Walker Lane-style dextral faulting directly south and east of the 3–D map suggests the possibility that some of the north- to north-northwest-striking 3–D mapped faults may have a component of dextral offset. However, in the absence of outcrop evidence for dextral displacement or obvious dextral offset of geophysical anomalies, all faults are mapped with pure normal offset.

Structure

The 3–D map illustrates a gently west-tilted half graben on the western limb of an extensional anticline. The axis of the extensional anticline is situated just east of the east margin of the 3–D map (figs. 6, 9). The geologic contact between the Miocene volcanic section (Tvs) and the Mesozoic crystalline basement (Mzu) within the half graben dips ~20–25° west. The westward tilting of the strata, rather than normal displacement across faults, accommodates the majority of the east-to-west deepening (from ~1.5 to 2.2 km) of the crystalline basement.

Forty-seven faults are defined within the map. The primary fault system strikes north- to north-northeast. These north-northeast-striking faults dip moderately (generally ~40–60°, though a few faults dip as much as ~72°) to the west; a secondary set of north-northeast-striking antithetic faults dip to the east (fig. 6, 10*I*). The north-northeast-striking, west-dipping fault system accommodates the westward tilting of the half graben. North- to north-northwest-striking and east-striking faults are also present, though the latter are statistically very minor (fig. 10*I*). The geometry of the fault system in the 3–D map (fig. 10*I*–10*J*) is consistent with the faults and fractures interpreted from borehole-image logs (Blake and Davatzes, 2012; Blake and others, 2015) in four wells from the Fallon FORGE site (fig. 10*A*–10*H*).

On the east side of the 3–D map near the hinge of the anticline, the density of faults is relatively high (for example, there are several faults per kilometer in the east-west direction), which is typical of the axial parts of extensional accommodation zones (for example, Faulds and Varga, 1998). This high density of faults is evidenced by relatively densely spaced, predominantly east dipping faults on the seismic-reflection profiles. This geometry is consistent with the observed gravity and magnetic anomaly data, especially the relatively high magnetic and gravity gradients evident on the maps (figs. 7, 8) and 2–D potential-field profile models (fig. 9). This extensional accommodation zone is likely an important structural control of fluid upwelling for the Carson Lake geothermal area, the name given to an approximately 5-km-long temperature anomaly with shallow (~215 m), warm (~120 °C) fluids to the south of the Fallon FORGE site (fig. 1; Ayling and others, 2018; Benoit, 1990).

To the west of the hinge zone, west-dipping and east-dipping normal faults are more widely spaced (~0.5–2.0 km perpendicular to strike). This is evident in the seismic-reflection data and the potential-field horizontal gradients (fig. 7, 8). The seismic-reflection data, in particular, and the relatively low gravity and magnetic gradients indicate that faults to the west of the hinge have relatively minor offset. Normal displacement across faults to the west of the hinge is tens of meters to 100 m.

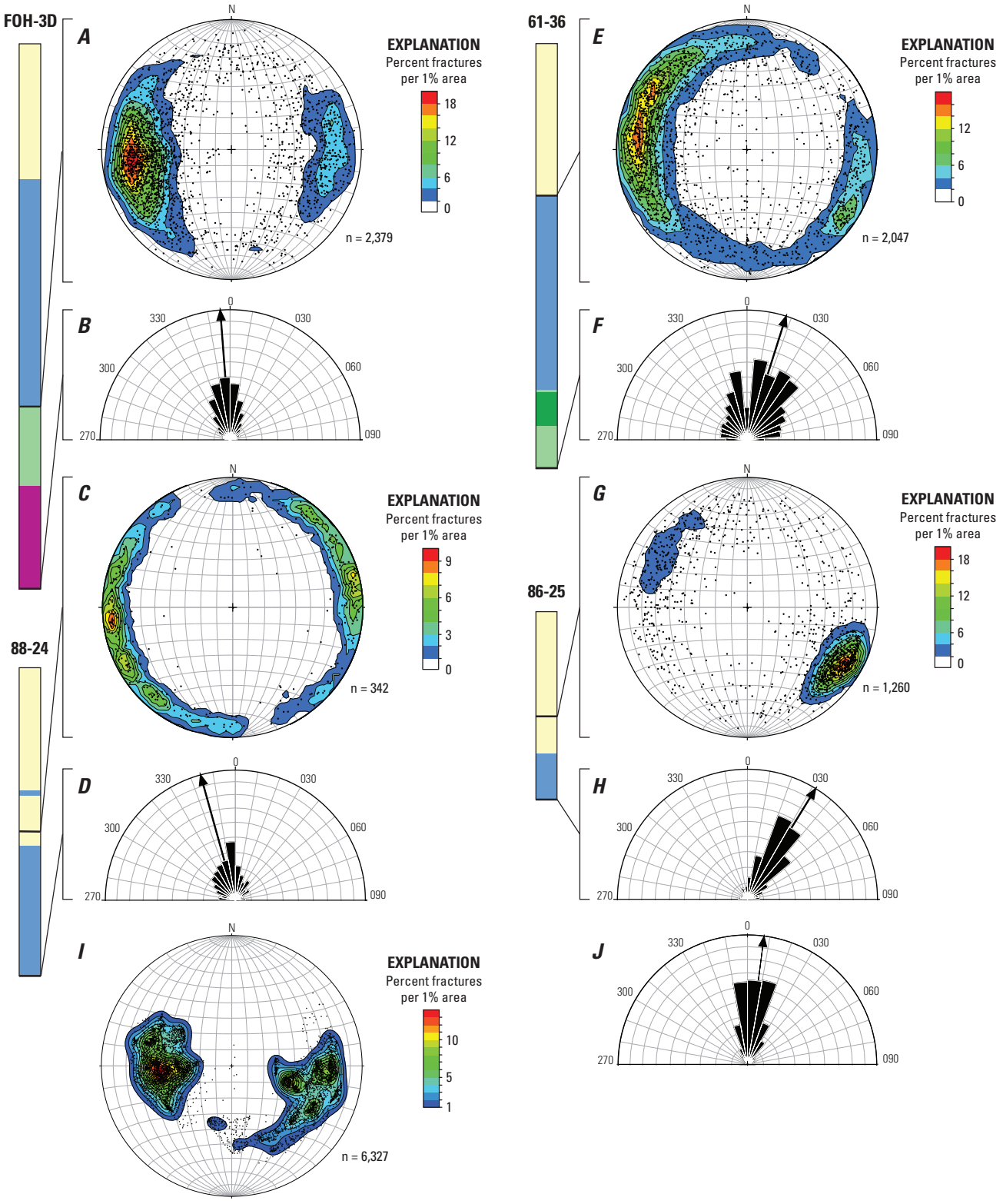

Figure 10. Lower hemisphere projections showing mapped faults and natural fractures in wells in the southern Carson Sink 3–D map area. Fractures in wells are interpreted from image logs: FOH-3–D, formation microscanner and acoustic borehole imager logs; 88-24, ultrasonic borehole imager log; 61-36, formation microimager log; 86-25, formation microimager log (Blake and Davatzes, 2012; Blake and others, 2015; Ayling and others, 2018). *A, C, E,* and *G*, Contoured poles to faults and fractures per 1 percent area. *B, D, F,* and *H,* Rose diagrams with mean arrows of strikes of natural fractures in wells FOH-3–D, 88-24, 61-36, and 86-25, respectively. Petals are 10° bins, and perimeter of the circle represents 30 percent of the data set. Lithologic logs (from fig. 3) indicate the section of these wells where natural fractures were picked. *I*, Poles to planes contoured at various intervals per 1 percent area. *J,* Rose diagram of fault strikes from 3–D geological map. Faults are subsampled at 200-m intervals along the 3–D surfaces. Petals represent 5° bins; the largest petal indicates that ~19 percent of fault segments strike between 11° and 15°, with a mean strike of 7 (N. 7° E.).

The Holocene and Pleistocene surface deposits and the inferred late Pliocene contact identified in seismic-reflection data constrain the relative ages of faulting in the 3–D map. All observed faults cut the contact between units Tvs and QTs, indicating offset as recent as Miocene. The general ~1 km constant thickness of unit Tvs (~16–12 Ma) suggests that subsidence of the half graben and the requisite faulting have largely occurred since ~12 Ma. Seven of the forty-seven faults are clearly observed to cut the inferred late Pliocene contact in the seismic-reflection profiles, indicating that these faults have offset as young as Pliocene. No evidence for late Pleistocene or younger surface faulting in the 3–D map area (Hinz and others, 2011; Bell and House, 2010; Bell and others, 2009; Morrison, 1964) suggests that the majority of the 3–D mapped fault system is as young as late Miocene to middle Pliocene, with several faults as young as late Pliocene to early Pleistocene.

Potential Applications for 3–D Map

In addition to geological characterization associated with enhanced geothermal systems (EGS) activities, the southern Carson Sink 3–D geologic map may be used for a variety of purposes.

Reservoir Modeling

The southern Carson Sink 3–D map is centered on and surrounds the Fallon FORGE site, which was the focus of EGS technologies and techniques as part of the U.S. Department of Energy FORGE study. This 3–D map provides the geologic baseline for modeling fluid stimulation and EGS reservoir characteristics associated with these activities (Ayling and others, 2018). Reservoir modeling constrains the locations, volumes, and rates of fluid to be injected and retrieved for potential electricity production while also describing the mechanical, thermal, and (or) hydrological effects that occur in the modeled EGS reservoir as a result of stimulation (Finstere and others, 2014; Kim and others, 2015).

Seismicity Analysis

The 3–D geologic map provides data on the natural fault system within the map area, including fault orientations, fault lengths, and the spatial distribution of faults. This information may be paired with local seismicity data and the location of sensitive infrastructure to evaluate the hazard and risk associated with natural seismicity or induced seismicity that may result from EGS activities (for example, Kaven and others, 2019). The 3–D map data may also be used as a baseline for characterizing the dynamic seismic response to EGS stimulation in the subsurface (Ayling and others, 2018).

Conventional Geothermal Exploration

The greater Carson Sink hosts eight known geothermal systems, six that currently produce electricity (fig. 1; Faulds and others, 2006, 2011, 2015). Conventional geothermal systems in the western United States, including those in and around the Carson Sink, commonly occur at discontinuities along faults (Curewitz and Karson, 1997; Faulds and others, 2006, 2011). These areas have inherent structural complexity exemplified by a high local density of interconnected faults and fractures. Permeability is greater in these faulted areas, which is beneficial for the development and maintenance of pathways for upwelling geothermal fluids (Siler and others, 2018b). Extensional accommodation zones (Faulds and Varga, 1998) provide one type of structural discontinuity that hosts many geothermal systems that have been developed for electricity production and many more known, but as yet undeveloped, systems (Faulds and others, 2013). The faults near the hinge of the anticlinal accommodation zone displayed in the eastern portion of the 3–D map are probably associated with geothermal upwelling associated with the Carson Lake geothermal system (fig. 1; Desormier, 1997). The 3–D map provides a detailed representation of the complex subsurface architecture of faults within the accommodation zone, which provides a context for understanding the geologic and tectonic factors that control permeability generation and geothermal fluid flow in this setting and in analogous settings.

Education and Scientific Inquiry

A 3–D geologic map supplements the information provided in 2–D geologic maps by allowing the user to visualize complex geologic relations in three dimensions. Geologic features may be viewed from different angles, and slices through the map may illustrate geologic relations along cross sections of any orientation. The complex spatial relations generated by faulting, folding, erosion, sedimentation, and other geologic processes may be visualized relatively quickly and easily, making 3–D geologic maps useful interpretive tools and teaching aids. This 3–D map may be used by the academic community and by the public to visualize the subsurface geologic relations present in the southern Carson Sink.

Basin Hydrogeology

Groundwater resources associated with both agricultural irrigation and drinking water are critical to the sustainability of many public and governmental interests in arid parts of the western United States, including the Basin and Range region. The 3–D geologic map provides information that is applicable to the assessment and management of water resources in the map area. Both sedimentary and volcanic rocks can be important aquifers in the Carson Sink (Glancy, 1986; Maurer and Welch, 2001). Faults and basin structures, which are shown in the map, control the distribution of sedimentary and volcanic aquifers. The local tectonic setting effects the types of processes that redistribute sediment and control grain-size distribution and, therefore, physical properties like porosity and permeability related to groundwater storage and transport. Local tectonics also influence the locations, facies, and aquifer potential of volcanic rocks.

Acknowledgments

This research was funded from 2015 to 2018 by a Department of Energy grant EE0007160 awarded to the Fallon FORGE team, with Sandia National Laboratory as lead on the project. Supplementary funding came from the Energy Program of the U.S. Geological Survey (USGS). We wish to thank the U.S. Navy for their cooperation and fruitful discussions, especially Commanding Officer, Captain David B. Halloran, and Public Works Officer, Commander Scott Beyer, at the Naval Air Station Fallon and the entire Fallon FORGE team, of which the authors are a small subset. We also thank Geoff Phelps at the USGS for managing the potential-fields database. We also thank Don Sweetkind and Ben Melosh for their helpful reviews of the pamphlet, data, and map sheet.

DESCRIPTION OF MAP UNITS

UNCONSOLIDATED DEPOSITS

QTs **Surficial sediments and sedimentary rocks, undivided (Holocene, Pleistocene, and Pliocene)**—Light- to medium-gray silt to coarse sand with rounded grains of quartz, lithic fragments, feldspars, micas, and clay (ordered from most to least abundant). Locally interlayered with reworked tuffs. Rarely altered to clays and chlorite. Generally poorly lithified. Late Pliocene to Holocene. Based on stratigraphic position and mineralogy, includes Holocene and Pleistocene sedimentary units from Morrison (1964), Bell and others (2009), and Bell and House (2010). Generally less well lithified than sedimentary rocks (Ts), though this alone is insufficient to define the contact. Distinguished from unit Ts on the basis of lying above the inferred late Pliocene contact identified in seismic-reflection data (fig. 6)

Ts **Sedimentary rocks (late Pliocene to Miocene)**—Light- to medium-gray silt to coarse sand with rounded grains of quartz, lithic fragments, feldspars, micas, and clay (ordered from most to least abundant) in a carbonate-cemented lithic sandstone. Locally interlayered with reworked tuffs. Rarely altered to clays and chlorite. Generally better lithified than surficial sediments and sedimentary rocks (QTs), though this alone is insufficient to define the contact. Primarily distinguished from unit QTs because it lays below the inferred late Pliocene contact identified in seismic-reflection data (fig. 6)

BEDROCK

VOLCANIC ROCKS

Tvs **Volcanic rocks, undivided (Miocene)**—Basaltic andesite lavas (dominant), andesite, volcanic breccia, lithic tuff, and rhyolite and dacite that, based on stratigraphic position and mineralogy, correlate with units mapped in the Bunejug Mountains and Lahontan Mountains (Morrison, 1964; Bell and others, 2009; Bell and House, 2010; Hinz and others, 2011)

Basaltic andesite lavas. Dark-gray aphanitic and locally sparsely porphyritic basaltic-andesite flows. Phenocrysts include mostly plagioclase and lesser olivine and pyroxene. Chlorite, calcite, and clay alteration is fairly common, as well as trace epidote and pyrite alteration. Quartz and calcite veins distributed sparsely throughout this unit. The most extensive Miocene volcanic unit in 3–D map area and correlates with unit Tba of Hinz and others (2011) exposed in Bunejug Mountains and unit Trb of Bell and others (2009) exposed in eastern Lahontan Mountains. Units Tba and Trb are dated at ~16 to 12 Ma (Hinz and others, 2011, 2014, unpublished data; Bell and others, 2009)

Andesite. Medium- to light-gray, sparsely porphyritic andesite flows with phenocrysts of pyroxene as long as 1 mm. Groundmass is aphanitic and glassy. Interlayered in unit Tba of Hinz and others (2011) in well 18-5 (fig. 2)

Volcanic breccia. Polymict, subrounded to subangular clast-dominated breccia. Mafic volcanic clasts include porphyritic, aphanitic, or vesicular basaltic andesite. Interlayered in unit Tba of Hinz and others (2011) in well 18-5 (fig. 2). Clast size ranges from 1 mm to 10 cm

Lithic tuff. Medium- to dark-gray tuff containing sparsely dispersed lithic fragments (locally reworked as a mudflow deposit) and a crystal-rich matrix. Interlayered in unit Tba of Hinz and others (2011) in wells 84-31 and 18-5 (fig. 2)

Rhyolite and dacite. Light-gray, sparsely to moderately porphyritic rhyolite and dacite lavas. Probably correlates with dacite (unit Trd of Bell and others, 2009) mapped in Lahontan Mountains quadrangle and rhyolite (unit Tr of Hinz and others, 2011; age ~12 Ma) mapped in Bunejug Mountains quadrangle. Interlayered in upper part of unit Tba of Hinz and others (2011) in wells 21-31 and 84-31 (fig. 2)

MESOZOIC CRYSTALLINE BASEMENT

Mzu **Metamorphic and plutonic rocks, undivided (Cretaceous, Jurassic, and Triassic)**—Undivided lithostratigraphic unit consisting of Cretaceous or Jurassic quartz monzonite (Mzqm), Jurassic metabasalt (Mzb), Jurassic quartzite with lesser matabasalt (Mzq), and Jurassic or Triassic metarhyolite (Mzr). Undivided in the 3–D map, but divided in the Fallon FORGE area part of the 3–D map into the following lithologic units:

Mzqm **Quartz monzonite (Cretaceous or Jurassic)**—White, fine- to medium-grained quartz monzonite identified in wells 82-36 and 21-31 (fig. 2). Weak to moderate chlorite alteration with calcite and trace prehnite in voids. Given that the quartz monzonite exposed in well 82-36 intrudes the metabasalt that rests on the Jurassic quartzite, this quartz monzonite is either Jurassic or Cretaceous. This is consistent with the pattern that most plutons exposed in the Carson Sink region are Jurassic to Cretaceous, with only a few Triassic plutons across the region. Overall, these Cretaceous and Jurassic granitic units are typical of western Nevada and formed in the back-arc region of the Sierran arc (for example, Oldow, 1984; Busby-Spera, 1988; Lutz and Hulen, 2002; Wyld, 2002)

Mzb **Metabasalt (Jurassic)**—Gray-green, aphanitic to fine-grained metabasalt to metabasaltic andesite (fig. 5); moderately to highly altered to clay and chlorite. Some sections are mottled red to purple. Less commonly, epidote and pyrite occur as alteration minerals. May correlate with Jurassic metabasalt exposed in Stillwater Range, ~60 to 100 km northeast of the 3–D map area (fig. 1; Page, 1965; Speed, 1976; John and Silberling, 1994)

Mzq **Quartzite with lesser phyllite, metabasalt, and marble (Jurassic)**—White to light-gray to pale-green quartzite with trace interstitial calcite; chlorite-pyrite alteration. Locally interlayered with dark-gray phyllite and slate, gray-green meta-andesite, and light-gray marble. Most likely correlates with the eolian Jurassic sandstone of the Boyer Ranch Formation (Page, 1965; Speed and Jones, 1969; Speed, 1976), though it is more metamorphosed than where the Boyer Ranch Formation is well exposed in the Stillwater Range. Boyer Ranch sandstone is interlayered with andesite lavas, marble, phyillite, and volcaniclastic sedimentary rocks at scales of 5 to 50+ m thicknesses in northern Stillwater Range (Lutz and Hulen, 2002). This interlayering is similar to the scale of layering intercepted in wells 61-36, FOH-3D, 82-36, and 21-31 at the Fallon FORGE site (fig. 2). Boyer Ranch sandstone is the only known major Mesozoic eolian sandstone in this region

Mzr **Metarhyolite with lesser metabasalt (Jurassic or Triassic)**—Metarhyolite with lesser meta-andesite. Pale-green, gray, and red mottled, abundantly to sparsely porphyritic rhyolite and ash-flow tuffs; altered devitrified matrix with trace to 1 percent pyrite and chlorite. Ash layers locally <3 m thick are interlayered with aphanitic meta-andesite. May correlate with Triassic rhyolite ash-flow tuffs interbedded with meta-andesite lavas and marine carbonates in Desert Mountains ~50 km southwest of 3–D map area (fig. 1; Hinz and others, 2013b). Similarly, in the Sand Springs Range ~40 km southeast of the 3–D map area, Triassic metarhyolite ash-flow tuffs are interbedded with carbonates and are intruded by multiple 237±5 Ma plutons (Satterfield, 2002). The most regionally extensive Triassic metarhyolite sequence is the ~225±30 Ma Rochester Rhyolite of the Koipato Group (Wallace and others, 1969; McKee and Burke, 1972; Silberling, 1973; Vikre, 1981), which is exposed in the Humboldt Range ~100 to 140 km north of 3–D map area, where it rests on meta-andesite and carbonate sequences. Jurassic metarhyolite ash-flow tuffs are also exposed in the central Stillwater Range ~50 km northwest of the 3–D map area (John, 1995).

References Cited

Anders, M.H., and Wiltschko, D.V, 1994, Microfracturing, paleostress and the growth of faults: Journal of Structural Geology, v. 16, p. 795–815, at https://doi.org/10.1016/0191-8141(94)90146-5.

Ayling, B., Blankenship, D., Sullivan, P., Kennedy, M., Majer, E.L., Villavert, M., Sonnenthal, E., Tang, J., Dobson, P., Hinz, N., Faulds, J., Hammond, W., Mlawsky, E., Blake, K., Tiedeman, A., Sabin, A., Lazaro, M., Akerley, J., Nordquist, J., Sophy, M., Siler, D.L., Ole Kaven, J., Phelps, G., Hickman, S., Glen, J., Williams, C., Robertson-Tait, A., Hackett, L., Pettitt, W., Riahi, A., Blanksma, D., Damjanac, B., Hazzard, J., Eneva, M., Witter, J.B., Queen, J., and Fortuna, M., 2018, Phase 2 update for the Fallon FORGE Site, Nevada, USA: Proceedings, Forty-third Workshop on Geothermal Reservoir Engineering, Stanford University, February 12–14, SGP-TR-213, 13 p.

Bell, J.W., Caskey, S.J., and House, P.K., 2009, Geologic map of the Lahontan Mountains quadrangle, Churchill County, Nevada: Nevada Bureau of Mines and Geology Map 168, scale 1:24,000, 1 sheet, 24 p.

Bell, J.W., and House, P.K., 2010, Geologic map of the Grimes Point quadrangle, Churchill County, Nevada: Nevada Bureau of Mines and Geology Map 173, scale 1:24,000, 1 sheet, 24 p.

Benoit, D., 1990, The Carson Lake Geothermal Prospect: unpublished Oxbow Power Corporation Report, 38 p.
Blackwell, D.D., Negraru, P.T., and Richards, M.C., 2007, Assessment of the Enhanced Geothermal System Resource Base of the United States: Natural Resources Research, v. 15, no. 4, p. 283–308, at https://doi.org/10.1007/s11053-007-9028-7.
Blake, K., and Davatzes, N.C., 2012, Borehole image log and statistical analysis of FOH-3D, Fallon Naval Air Station, NV: Proceedings, Thirty-Seventh Workshop on Geothermal Reservoir Engineering, Stanford University, 14 p.
Blake, K., Tiedeman, A., Sabin, A., Lazaro, M., Meade, D., and Huang, W-C., 2015, Naval Air Station Fallon mainside—Update of geothermal exploration: Geothermal Resources Council Transactions, v. 39, p. 407–414.
Blakely, R.J., 1995, Potential theory in gravity and magnetic applications: Cambridge, U.K., Cambridge University Press.
Blakely, R.J., and Connard, G.G., 1989, Crustal studies using magnetic data, chap. 4 *of* Pakiser, L.C., and Mooney, W.D., Geophysical Framework of the Continental United States: Geological Society of America Memoir 172, p. 45–60, at https://doi.org/10.1130/Mem172-p45.
Blankenship, D., Akerley, J., Blake, K., Calvin, W., Faulds, J.E., Glen, J.M.G., Hickman, S., Hinz, N., Kaven, O., Lazaro, M., Meade, D., Kennedy, B.M., Phelps, G., Sabin, A., Schoenball, M., Siler, D.L., Robertson-Tait, A., and Williams, C., 2016, Frontier Observatory for Research in Geothermal Energy—Phase 1 topical report, Fallon, NV: Sandia National Laboratories Report, SAND2016-8929, 311 p.
Busby-Spera, C.J., 1988. Speculative tectonic model for the early Mesozoic arc of the southwest Cordilleran United States: Geology, v. 16, no. 121, p.1121–1125, at https://doi.org/10.1130/0091-7613(1988)016%3C1121:STMFTE%3E2.3.CO;2.
Caskey, S.J., Bell, J.W., Ramelli, A.R., and Wesnousky, S.G., 2004, Historical surface faulting and paleoseismicity in the area of the 1954 Rainbow Mountain-Stillwater earthquake sequence, central Nevada: Bulletin of the Seismological Society of America, v. 94, no. 4, p. 1255–1275.
Colgan, J.P., Dumitru, T.A., Reiners, P.W., Wooden, J.L., and Miller, E.L., 2006, Cenozoic tectonic evolution of the Basin and Range Province in northwestern Nevada: American Journal of Science, v. 306, p. 616–654, at https://doi.org/10.2475/08.2006.02.
Cousens, B.L., Prytulak, J., Henry, C.D., Alcazar, A., and Brownrigg, T., 2008, The geology, geochronology and geochemistry of the Miocene–Pliocene ancestral Cascades Arc, northern Sierra Nevada, California/Nevada; the roles of the upper mantle, subducting slab, and the Sierra Nevada lithosphere: Geosphere, v. 4, p. 829–853.
Cowie, P.A., and Scholz, C.H., 1992, Displacement-length scaling relationship for faults; data synthesis and discussion: Journal of Structural Geology, v. 14, no. 10, p. 1149–1156.
Crafford, A.E.J., 2010, Geologic terrane map of Nevada: Nevada Bureau of Mines and Geology Open-File Report OF104, 1 CD-ROM, 46 p., 2 plates.
Curewitz, D., and Karson, J.A., 1997, Structural settings of hydrothermal outflow; fracture permeability maintained by fault propagation and interaction: Journal of Volcanology and Geothermal Research, v. 79, p. 149–168, at https://doi.org/10.1016/S0377-0273(97)00027-9.
Davatzes, N.C., and Hickman, S., 2010, The feedback between stress, faulting, and fluid flow—Lessons from the Coso Geothermal Field, CA, USA: Proceedings, World Geothermal Congress 2010, 14 p.
Desormier, 1997, A case study of the Carson Lake geothermal project at Carson Lake, Nevada: Proceedings, Twenty-First Workshop on Geothermal Reservoir Engineering, Stanford University, p. 105–112.
Doser, D.I., 1986, Earthquake processes in the Rainbow Mountain-Fairview Peak-Dixie Valley, Nevada, region, 1954–1959: Journal of Geophysical Research: v. 91, p. 12572–12586.
Faulds, J.E., Blankenship, D., Hinz, N.H., Sabin, A., Nordquist, J., Hickman, S., Glen, J., Kennedy, M., Robertson-Tait, A., Williams, C., and Calvin, W., 2015, Geologic setting of the proposed Fallon FORGE site, Nevada—Suitability for EGS research and development: Geothermal Resources Council Transactions, v. 39, p. 293–301.
Faulds, J.E., Coolbaugh, M.F., Benoit, D., Oppliger, G., Perkins, M., Moeck, I., and Drakos, P., 2010a, Structural controls of geothermal activity in the northern Hot Springs Mountains, western Nevada—The tale of three geothermal systems (Brady's, Desert Peak, and Desert Queen): Geothermal Resources Council Transactions, v. 34, p. 675–683.
Faulds, J.E., Coolbaugh, M.F., Vice, G.S., and Edwards, M.L., 2006, Characterizing structural controls of geothermal fields in the northwestern Great Basin—A progress report: Geothermal Resources Council Transactions, v. 30, p. 69–76.
Faulds, J.E., and Henry, C.D., 2008, Tectonic influences on the spatial and temporal evolution of the Walker Lane—An incipient transform fault along the evolving Pacific-North American plate boundary, *in* Spencer, J.E., and Titley, S.R., eds., Ores and orogenesis—Circum-Pacific tectonics, geologic evolution, and ore deposits: Arizona Geological Society Digest, v. 22, p. 437–470.
Faulds, J.E., and Hinz, N.H., 2015, Favorable tectonic and structural settings of geothermal systems in the Great Basin region, western USA—Proxies for discovering blind geothermal systems: Proceedings, World Geothermal Congress, Melbourne, Australia, 19–25 April, 6 p.
Faulds, J.E., Hinz, N.H., Coolbaugh, M.F., Cashman, P.H., Kratt, C., Dering, G.M., Edwards, J., Mayhew, B., and Mclachlan, H., 2011, Assessment of favorable structural settings of geothermal systems in the Great Basin, western USA: Geothermal Resources Council Transactions, v. 35, p. 777–784.
Faulds, J.E., Hinz, N.H., Dering, G.M., and Siler, D.L., 2013, The hybrid model—The most accommodating structural setting for geothermal power generation in the Great Basin, western USA: Geothermal Resources Council Transactions, v. 37, p. 4–10.
Faulds, J.E., Hinz, N.H., and Kreemer, C.W., 2012, Regional patterns of geothermal activity in the Great Basin region,

western USA—Correlation with strain rates: Geothermal Resources Council Transactions, v. 36, p. 897–902.
Faulds, J.E., Hinz, N.H., Siler, D.L., Glen, J.M., Fortuna, M.A., Queen, J.H., and Blake, K., 2018, Update on the stratigraphic and structural framework of the proposed Fallon FORGE site, Nevada: Geothermal Resources Council Transactions, v. 42, p. 1026–1046.
Faulds, J., Moeck, I., Drakos, P., and Zemach, E., 2010b, Structural assessment and 3–D geological modeling of the Brady's Geothermal Area, Churchill County (Nevada, USA)—A preliminary report: Proceedings, Thirty-Fifth Workshop on Geothermal Reservoir Engineering, Stanford University, February 1–3, SGP-TR-188, 5 p.
Faulds, J.E., and Varga, R., 1998, The role of accommodation zones and transfer zones in the regional segmentation of extended terranes: Geological Society of America Special Paper 323, p. 1–46.
Finsterle, S., Sonnenthal, E.L., and Spycher, N., 2014, Advances in subsurface modeling using the TOUGH suite of simulators: Computers & Geosciences, v. 65, p. 2–12.
Fosdick, J.C., and Colgan, J.P., 2008, Miocene extension in the East Range, Nevada—A two-stage history of normal faulting in the northern Basin and Range: Geosphere, v. 120, no. 9/10, p. 1198–1213.
Glancy, P.A., 1986, Geohydrology of the basalt and unconsolidated sedimentary aquifers in the Fallon area, Churchill County, Nevada: U.S. Geological Survey Water-Supply Paper 2263, 70 p.
Gray, B., Unruh, J., Bjornstad, S., Blake, K., Alm, S., and Shoffner, J., 2013, Targeting geothermal resources in the Lahontan Valley, Nevada; analysis of Neogene faulting through 2–D seismic, topographic, and satellite imagery analysis: Geothermal Resources Council Transactions, v. 37, p. 1013–1018.
Hastings, D.D., 1979, Results of exploratory drilling northern Fallon basin, western Nevada: Rocky Mountain Association of Geologists and Utah Geological Association, Basin and Range Symposium and Great Basin Field Conference, p. 515–522.
Henry, C.D., 2008, Ash-flow tuffs and paleovalleys in northeastern Nevada—Implications for Eocene paleogeography and extension in the Sevier hinterland, northern Great Basin: Geosphere, v. 4, no. 1, p. 1–35, at https://doi.org/10.1130/GES00122.1.
Henry, C.D., Hinz, N.H., Faulds, J.E., Colgan, J.P., John, D.A., Brooks, E.R., Cassel, E.J., Garside, L.J., Davis, D.A., and Castor, S.B., 2012, Eocene–early Miocene paleotopography of the Sierra Nevada-Great Basin-Nevadaplano based on widespread ash-flow tuffs and paleovalleys: Geosphere, v. 8, no. 1, p. 1–27, at https://doi.org/10.1130/GES00727.1.
Hinz, N.H., Faulds, J.E., and Bell, J.W., 2011, Preliminary geologic map of the Bunejug Mountains quadrangle, Churchill County, Nevada: Nevada Bureau of Mines and Geology Open-File Report 11-9, 1 sheet, scale 1:24,000.
Hinz, N.H., Faulds, J.E., and Coolbaugh, M.F., 2014, Association of fault terminations with fluid flow in the Salt Wells geothermal field, Nevada, USA: Geothermal Resources Council Transactions, v. 38, p. 3–9.
Hinz, N.H., Faulds, J.E., Glen, J.M.G., Siler, D.L., Queen, J., Witter, J.B., Tiedeman, A., Blake, K., and Blankenship, D., 2017, Fallon FORGE—Analog geologic studies, reanalysis of 2–D seismic profiles, and new potential fields geophysics studies: Geothermal Resources Council Transactions, v. 41, p. 300.
Hinz, N.H., Faulds, J.E. and Oppliger, G.L., 2008, Structural controls of Lee-Allen Hot Springs, southern Churchill County, western Nevada—A small pull-apart in the dextral shear zone of the Walker Lane: Geothermal Resources Council Transactions, v. 32, p. 285–290.
Hinz, N.H., Faulds, J.E., and Oppliger, G.L., 2010, Preliminary geologic map of the Lee-Allen geothermal area, Churchill County, Nevada: Nevada Bureau of Mines and Geology Open-File Report 10-6, 1 sheet, scale 1:24,000 with scale 1:8,000 inset.
Hinz, N.H., Faulds, J.E., and Siler, D.L., 2013a, Developing systematic workflow from field work to quantitative 3–D modeling for successful exploration of structurally controlled geothermal systems: Geothermal Resources Council Transactions, v. 37, p. 275–279.
Hinz, N.H., Faulds, J.E., Siler, D.L., Tobin, B., Blake, K., Tiedeman, A., Sabin, A., Blankenship, D., Kennedy, M., Rhodes, G., Nordquist, J., Hickman, S., Glen, J., Williams, C., Robertson-Tait, A., and Calvin, W., 2016, Stratigraphic and structural framework of the proposed Fallon FORGE site, Nevada: Proceedings, Forty-first Workshop on Geothermal Reservoir Engineering, Stanford University, Feb. 22–24, 12 p.
Hinz, N.H., Ramelli, A.R., and Faulds, J.E., 2013b, Preliminary geologic map of the Wabuska quadrangle, Lyon County, Nevada: Nevada Bureau of Mines and Geology Open-File Report 13-08, 1 sheet, scale 1:24,000.
Jachens, R.C., and Moring, B.C., 1990, Maps of the thickness of Cenozoic deposits and the isostatic residual gravity over basement for Nevada: U.S. Geological Survey Open-File Report 90–404.
John, D.A., 1995, Tilted middle Tertiary ash-flow calderas and subjacent granitic plutons, southern Stillwater Range, Nevada—Cross sections of an Oligocene igneous center: Geological Society of America Bulletin, v. 107, p. 180–200.
John, D.A., and Silberling, N.J., 1994, Geologic map of the La Plata Canyon quadrangle, Churchill County, Nevada: U.S. Geological Survey Geologic Quadrangle Map GQ–1710.
Jolie, E., Faulds, J.E., and Moeck, I., 2012, The development of a 3–D structural-geological model as part of the geothermal exploration strategy—A case study from the Brady's geothermal system, Nevada, USA: Proceedings, Thirty-Seventh Workshop on Geothermal Reservoir Engineering, Stanford University, p. 421–425.
Jolie, E., Moeck, I., and Faulds, J.E., 2015, Quantitative structural-geological exploration of fault-controlled geothermal systems—A case study from the Basin-and-Range Province, Nevada (USA): Geothermics, v. 54, p. 54–67, at https://doi.org/10.1016/j.geothermics.2014.10.003.
Kaven, J.O., Majer, E.L., Foxall, W., Sonnenthal, E.L., and Pettitt, W., 2019, Seismic hazard assessment at the Fallon, Nevada, Frontier Observatory for Research in Geother-

mal Energy Site (No. 2019-1020): U.S. Geological Survey Open-File Report 2019–10020, at https://doi.org/10.3133/ofr20191020.

Kim, J., Sonnenthal, E. and Rutqvist, J., 2015, A sequential implicit algorithm of chemo-thermo-poro-mechanics for fractured geothermal reservoirs: Computers & Geosciences, v. 76, p. 59–71.

Lutz, S.J., and Hulen, J.B., 2002, Geologic setting and alteration mineralogy of the Nickel Mine and Bolivia region, Jurassic Humboldt mafic complex and Boyer Ranch Formation, northern Stillwater Range, Nevada: Geologic Society of Nevada Special Publication 35, Spring 2002 Field Trip Guidebook, p. 117–127.

Maurer, D.K., and Welch, A.H., 2001, Hydrogeology and geochemistry of the Fallon basalt and adjacent aquifers, and potential sources of basalt recharge, in Churchill County, Nevada: U.S. Geological Survey Water-Resources Investigations Report 01-4130, 2 sheets, 72 p.

McKee, E.H., and Burke, D.B., 1972, Fission-track age bearing on the Permian-Triassic boundary and time of the Sonoma Orogeny in north-central Nevada: Geological Society of America Bulletin, v. 83, no. 7, p. 1949–1952.

Moeck, I., Hinz, N., Faulds, J.E., Bell, J.W., Kell-Hills, A., and Louie, J., 2010, 3–D geological mapping as a new method in geothermal exploration—A case study from central Nevada: Geothermal Resources Council Transactions, v. 34, p. 807–812.

Moeck, I., Kwiatek, G., and Zimmerman, G., 2009, Slip tendency analysis, fault reactivation potential and induced seismicity in a deep geothermal reservoir: Journal of Structural Geology, v. 31, p. 1174–1182, at https://doi.org/10.1016/j.jsg.2009.06.012.

Morrison, R.B., 1964, Lake Lahontan—Geology of southern Carson Desert, Nevada: U.S. Geological Survey Professional Paper 401, plates 3, 5.

Oldow, J.S., 1984, Evolution of a late Mesozoic back-arc fold and thrust belt, northwestern Great Basin, U.S.A: Tectonophysics, v. 102, no. 1–4, p. 245–274.

Page, B.M., 1965, Preliminary geologic map of part of the Stillwater Range, Churchill County, Nevada: Nevada Bureau of Mines and Geology Map 28, 1 sheet, 1:125,000 scale.

Phelps, G., and Glen, J.M., 2018, Geophysical datasets for the FORGE Fallon site: U.S. Geological Survey data release, https://doi.org/10.5066/F7J38RVZ.

Sandia National Laboratories, 2016, FORGE—Fallon, Nevada LiDAR Acquisition and Processing Report [data set]: Sandia National Laboratories, lidar data collection 10/9 to 12/4/2010, http://gdr.openei.org/submissions/821.

Sandia National Laboratories, 2017, Fallon, Nevada FORGE Gravity and Magnetics Data [data set]: Sandia National Laboratories, Geothermal Data Repository, http://gdr.openei.org/submissions/990.

Sandia National Laboratories, 2018a, Fallon, Nevada FORGE Lithology Logs and Well 21-31 Drilling Data [data set]: Sandia National Laboratories, Geothermal Data Repository, http://gdr.openei.org/submissions/1027.

Sandia National Laboratories, 2018b, Fallon, Nevada FORGE Seismic Reflection Profiles [data set]: Sandia National Laboratories, Geothermal Data Repository, http://gdr.openei.org/submissions/1011.

Satterfield, J.I., 2002, Geology map of the southern Sand Springs Range: Nevada Bureau of Mines and Geology Map 133, 1 sheet, scale 1:24,000 16 p.

Scholz, C.H., Dawers, N.H., Yu, J., Anders, M.H., and Cowie, P.A., 1993, Fault growth and fault scaling laws—Preliminary Results: Journal of Geophysical Research, v. 98, p. 951–961.

Schweickert, R.A., and Cowan, D.S., 1975, Early Mesozoic tectonic evolution of the western Sierra Nevada, California: Geological Society of America Bulletin, v. 86, p. 1329–1336.

Silberling, N.J., 1973, Geologic events during Permo-Triassic time along the Pacific margin of the United States, *in* Logan, A., and Hills, L.V., eds., International Permian-Triassic conference volume: Calgary, Alberta, Society of Petroleum Geologists, p. 345–362.

Siler, D.L., and Faulds, J.E., 2013, Three-dimensional geothermal fairway mapping—Examples from the western Great Basin, USA: Geothermal Resources Council Transactions, v. 37, p. 327–332.

Siler, D.L., Faulds, J.E., Mayhew, B., and McNamara, D.D., 2016a, Analysis of the favorability for geothermal fluid flow in 3–D, Astor Pass geothermal prospect, Great Basin, northwestern Nevada, USA: Geothermics, v. 60, p. 1–12, at https://doi.org/10.1016/j.geothermics.2015.11.002.

Siler, D.L., Hinz, N.H., and Faulds, J.E., 2018b, Stress concentrations at structural discontinuities in active fault zones in the western United States—Implications for permeability and fluid flow in geothermal fields: Geological Society of America Bulletin, v. 130, no. 7–8, p. 1273–1288, at https://doi.org/10.1130/B31729.1.

Siler D.L., Hinz, N.H., Faulds, J.E., Ayling, B., Blake, K., Tiedeman, A., Sabin, A., Blankenship, D., Kennedy, M., Rhodes, G., Sophy, M.J., Glen, J.M.G., Phelps, G.A., Fortuna, M., Queen, J., and Witter, J.B., 2018a, The geologic and structural framework of the Fallon FORGE site: Proceedings, Forty-Third Workshop on Geothermal Reservoir Engineering, Stanford University, 7 p.

Siler, D.L., Hinz, N.H., Faulds, J. E., and Queen, J., 2016b, 3–D analysis of geothermal fluid flow favorability, Brady's, Nevada, USA: Proceedings, Forty-First Workshop on Geothermal Reservoir Engineering, Stanford University, 10 p.

Siler, D.L., Hinz, N.H., Faulds, J.E., Tobin, B., Blake, K., Tiedeman, A., Sabin, A., Lazaro, M., Blankenship, D., Kennedy, M., Rhodes, G., Hickman, S., Glen, J., Williams, C., Robertson-Tait, A., and Pettitt, W., 2016c, The geologic framework of the Fallon FORGE site: Geothermal Resources Council Transactions, v. 40, p. 573–584.

Speed, R.C., 1976, Geologic map of the Humboldt Lopolith and surrounding terrane, Nevada: Geologic Society of America Map and Chart Series MC-14,

Speed, R.C., and Jones, R.A., 1969, Synorogenic quartz sandstone in the Jurassic mobile belt of western Nevada—Boyer Ranch Formation: Geological Society of America Bulletin, v. 80, p. 2551–2584.

Stewart, J.H., 1988, Tectonics of the Walker Lane belt, western Great Basin—Mesozoic and Cenozoic deformation in a zone of shear, *in* Ernst, W.G., ed., Metamorphism and crustal evolution of the western United States: Englewood Cliffs, New Jersey, Prentice-Hall, p. 683–713.

Stewart, J.H., and Carlson, J.E., 1978, Geologic map of Nevada: U.S. Geological Survey Miscellaneous Field Studies Map MF–930, 1:500,000 scale, 1 sheet.

Stockli, D.F., Surpless, B.E., Dumitru, T.A., and Farley, K.A., 2002, Thermochronological constraints on the timing and magnitude of Miocene and Pliocene extension in the central Wassuk Range, western Nevada: Tectonics, v. 21, no. 4, 21 p., at https://doi.org/10.1029/2001TC001295.

Talwani, M., Worzel, J.L., and Landisman, M., 1959, Rapid gravity computations for two-dimensional bodies with application to the Mendocino submarine fracture zone: Journal of Geophysical Research, v. 64, no. 1, p.49–59.

Telford, W.M., Geldart, L.P., and Sheriff, R.E., 1990, Applied geophysics (2d ed.): Cambridge, U.K., Cambridge University Press.

Tester, J.W., Anderson, B.J., Batchelor, A.S., Blackwell, D.D., DiPippp, R., Drake, E.M., Garnish, J., Livesay, B., Moore, M.C., Nichols, K., Petty, S., Toksöv, M.N., Veatch, R.W.J., Baria, R., Augustine, C., Murphy, E., Negraru, P., and Richards, M., 2006, The future of geothermal energy—Impact of enhanced geothermal systems (EGS) on the United States in the 21st century: Cambridge, Massachusetts Institute of Technology, 372 p.

U.S. Geological Survey, 2006, Quaternary fault and fold database of the United States: accessed 5/1/16, at https://earthquake.usgs.gov/hazards/qfaults/.

Vikre, P.G., 1981, Silver mineralization in the Rochester district, Pershing County, Nevada: Economic Geology, v. 76, no. 3, p. 580–609.

Wallace, R.E., Silberling, N.J., Irwin, W.P., and Tatlock, D.B., 1969, Geologic map of the Buffalo Mountain quadrangle: U.S. Geological Survey Geologic Quadrangle Map GQ–821, scale 1:62,500.

Wernicke, B.P., England, P.C., Sonder, L.J., and Christiansen, R.L., 1987, Tectonomagmatic evolution of Cenozoic extension in the North American Cordillera: The Geological Society of London, Special Publications, v. 28, p. 203–221, at https://doi.org/10.1144/GSL.SP.1987.028.01.15.

Williams, C.F., Reed, M.J., Mariner, R.H., DeAngelo, J., and Galanis, S.P.J., 2008, Assessment of moderate- and high-temperature geothermal resources of the United States: U.S. Geological Survey Fact Sheet 2008–3082, 4 p.

Witter, J.B., Glen, J.M.G., Siler, D.L., and Fournier, D., 2018, 2–D and 3–D potential field mapping and modelling at the Fallon FORGE site, Nevada, USA: Geothermal Resources Council Transactions, v. 42, p. 1194–1214.

Wyld, S.J, 2002, Structural evolution of a Mesozoic backarc fold-and-thrust belt in the U.S. Cordillera—New evidence from northern Nevada: Geological Society of America Bulletin, v. 114, no. 11, p. 1452–1468.